Final Scientific Report

SC0001986-1

Award No.: DE-SC0001986
Development and Pilot Manufacture of Pseudo-Electric Double Layer Capacitors

September 29-2009-September 28, 2010

The Research Foundation of State University of New York
Binghamton University
PO Box 6000
Binghamton, New York 13902-6000

Principal Investigator: Bahgat Sammakia
Professor, Department of Mechanical Engineering
Binghamton University
PO Box 6000
Binghamton, New York 13902-6000

Team Member:
Ioxus, Inc.
Winney Hill Road
Oneonta, New York

Report Author:
Dae Young Jung
Senior Scientist
The Small Scale Systems Integration and Packaging Center
Binghamton University
Binghamton, NY 13902-6000

TABLE OF CONTENTS **Page**

I. Executive Summary **3**

II. Accomplishments **4**

III. Project Activities **5**

A. Thermal Modeling for a Single Cell **6**
B. Thermal Modeling for Clustered Cells **24**
C. Materials Characterization and Formulation Optimization Study **30**
D. Ioxus Subawardee Activities **45**

IV. Project Developed and Technology Transfer **49**

I. Executive Summary

Binghamton University and Ioxus, a company located in Oneonta, New York, collaborated on the development of a third-generation EDLC (electric double layer capacitor) device also known as a P-EDLC or pseudo ELDC. ELDC is also known as supercapacitor due to its extremely high capacitance value, compared to conventional capacitors. Ioxus operates an EDLC manufacturing plant in Oneonta, New York that produces traditional EDLC devices with capacitance ratings up to 5000 F and would like to expand operations to include the manufacture of P-EDLC devices.

The company produced some P-EDLC devices on an experimental basis; however the devices were not optimal in terms of their potential (energy and power densities) and were of low capacitance in the range of about 200F. Thus the project focused on the characterization of the devices including the specific chemistry associated with the processes taking place in the device and how those chemical aspects of the device influence the electrical characteristics of the device. The development program also included the design and creation of prototype equipment to build the devices using a technology developed by the company over past years.

Binghamton University carried out basic studies on thermal characteristics of the current ELDC design and characterization of current active and conductive carbon materials used to fabricate ELDC and p-ELDC. Multi physics approach was take for thermal modeling to understand the temperature distribution of an individual cell as well as multi-cell systems, which is an important factor to the reliability of ELDC's and p-ELDC's. Structure and properties were characterized for various raw active carbon materials which can be used as electrode to look into potential cost reduction opportunity without degrading the performance. BU team also performed experiments for compositional optimization studies for active carbon, conductive carbon, and binder formulation. A few laboratory instruments were installed for this project at BU. These instruments will continued to be used to carry out further research and development tasks relevant to ELDC and p-ELDC.

Ioxus successfully created, enhanced, and then generated a product line of hybrid capacitors which now range in size from 220 Farads (F) to 1000F. These products have been proven to work as the primary energy storage method for LED lighting applications, and two significant commercial applications are evaluating these devices for use. Both of these applications will be used in LED lighting, which replaces traditional batteries and allows for a very fast charge and a high cycle life, over a wide temperature range. This will lead to a significant reduction of waste that ends up in landfills. These products are 70% recyclable, with a 10 year life. In one both applications, it is expected that the hybrid capacitor will power the LED lights for the life of the product, which would have required at least 10 battery changes.

II. Accomplishments

Binghamton University team developed a coupled electrochemical and thermal multi-dimensional model for studying the electrochemical behavior and thermal management of supercapacitors. Various parameters such as the electrolyte concentration, cell voltage, and heat generation rate in supercapacitor cells were examined. The electrochemical behavior of the supercapacitor cell under different discharge/charge rates and porosities in the electrode were investigated. In thermal model, core region is simplified by adopting the average properties, and the contact layer and the metal case are all included. The thermal model included the location-dependent convection and radiation heat transfer simultaneously to enhance the accuracy at the boundaries. From the modeling result, it was shown that the maximum temperature increases significantly with increasing the discharge rate whereas the temperature uniformity decreases with the discharge rate. The temperature distribution within the supercapacitor showed that heat transfer is greater in Y and Z directions than in X direction. It also showed that the metal case and the contact layer are important components. Furthermore, radiation is found to be an important process for heat dissipation, especially in situations under natural convection. Applied strong forced convection on all surfaces is effective in depressing the maximum temperature inside the supercapacitor, but it decreases the uniformity and impairs the supercapacitor performance. Results from the simulation show if just applying forced convection on Y direction surfaces and increasing the contact layer thermal conductivity, the temperature gradient in supercapacitors will become more uniform, because of higher thermal conductivity in Y direction. Finally, the results obtained with this numerical model can be used to determine the cooling system required for actual supercapacitor applications.

Various carbon materials for electrode were characterized to obtain the most suitable active carbon for electrode preparation. Electrode prototype was prepared with these selected materials. In the first step the capacitance measuring technique was established from which behavior of electrode was predicted for different composition. The capacitance value increased with increase in conductive carbon wt. percentage from 5 to 7% and then decreased as we increased the number further. This showed that the electrode composition of 7 % conductive carbon was the ideal one showing efficient charge discharge characteristics. Various carbon materials and new nano size carbon materials such as carbon nano tubes need to be further investigated as potential electrode material to increase the capability of energy storage and performance enhancement.

Through DOE funding, Ioxus successfully created, enhanced, and generated a product line of hybrid capacitors with range from 220 Farads (F) to 1000F. These products demonstrated its capability as energy storage method for LED lighting applications. Two other potential applications are being evaluated for these devices. Both of these applications can replace traditional batteries. This will lead to a significant reduction of waste that ends up in landfills. These products are 70% recyclable, with a 10 year life. In one both applications, it is expected

that the hybrid capacitor will power the LED lights for the life of the product, which would have required at least 10 battery changes.

III. Project Activities

Introduction

This project reflects research collaboration between The Small Scale Systems Integration and Packaging Center (S^3IP), a New York State Center of Excellence located at Binghamton University, and Ioxus, Inc., a New York State Corporation located on Oneonta, New York, that builds electric double layer capacitors. S^3IP develops new electronic applications to enhance the way people live and interact with their surroundings. An academic-industry-government partnership, the Center provides the microelectronics industry with solutions for challenges and opportunities in small scale systems design—development, prototyping process development, integration, packaging and manufacturing. The Center performs high-impact basic and applied research to support the successful technical translation of economically significant innovations such as electronics systems integration, new materials and sensors, new flexible electronic manufacturing technologies and modeling, analysis and characterization to national industry sectors.

The Center has developed the expertise and infrastructure to assist industry with their analytical and experimental modeling, specifically, verified predictive modeling, needs. Predictive verified models are a key aspect of applied research which enables the development of new materials, designs and new products. Models also aid system and product optimization and play a key role in technology transfer and commercialization by speeding up product development cycles, accurately predicting product life and reducing cost. However for modeling to be integrated into the research and development cycle, it is important to develop accurate material property data sets and to verify all modeling assumptions and simplifications through precise representative experimental measurements. S^3IP is a leader in establishing the necessary infrastructure (people, instrumentation and expertise) to measure material properties accurately. Unique and specialized testing laboratories include the Analytical and Diagnostics Laboratory, Nano indentation (Frances et al, 2004), Moiré interferometry (Park et al, 1997) (Park et al, 1999), drop testing and shock and vibration (Hontae et al, 2005) (Pitarresi et al, 2004) and modified atomic force microscopy to measure thermal conductivity at the nano scale (Desai et al, 2004) (Mahajan, 2007) (Desai et al, 2006) well as many others. The center also has a extensive stress testing and failure analysis laboratory capable of conducting most of the necessary tests for qualifying electronic systems including thermal and humidity cycling, high cycle fatigue testing, vibrations and drop testing enabling advanced reliability modeling (Chaparala et al, 2005). All of these capabilities enable the center to perform analyses that are fully verified and predictive in many areas of emerging technology such as nano structured materials, three dimensional Silicon systems, and

MEMS based interconnect systems for 3D packages (Acklet et al, 2006) (Desai et al, 2007) (Desai et al, 2007a).

The Center has been pleased to partner with Ioxus, Inc. on the development of high energy density electric double layer capacitors. Ioxus currently manufactures traditional electric double layer capacitors (EDLC) and has developed a second generation device that has high energy density. The higher energy density coupled with the device's characteristic high power density would make these devices a crucial component in any energy storage or power quality application. This collaborative research program focused on improvement of the activated, carbon addition of high dielectric materials, and development of proprietary electrolyte materials, and thermal modeling of a supercapacitor cell and clustered cells. The program goal was to provide basic understanding of materials used in supercapacitors, their themal dissipation aspects, and develop a hybrid EDLC, an electric double layer capacitor with an electrochemical component.

A. Thermal Modeling for a Single Cell: Multiphysics approach to modeling super capacitors for improving performance

1. Introduction:

Supercapacitors have been an active research area during recent years owing to their very high specific power, short discharge-time operation, high cycle efficiency, and good reversibility[1-3]. Supercapacitors have very high but not 100% cycle efficiency, so they do have energy lose. During the charge and discharge processes, especially at high current densities, current flowing through the supercapacitor structure causes internal heat generation and then results in undesirable overheating and temperature gradient. Enhancement with respect to performance, reliability and safety of supercapacitors needs a better understanding of electrochemical-thermal mechanism.

Although experiments[4-9] are necessary to obtain supercapacitor thermal data for design and optimization, thermal modeling is an effective way to provide valuable internal information to help optimize the supercapacitor in a cost-effective method. Until now, a number of models have been developed for analyzing the performance of supercapacitors. The double layer charging phenomenon was first modeled by Posey and Morozumi[10]. Then the performance of a supercapacitor cell was studied in detail by Pillay and Newman[11]. Later, Srinivasan and Weidner[12] presented an one dimensional analytical solution for the performance of a supercapacitor cell under constant current operation. In these models, electrolyte concentration was neglected, and the physical properties of the supercapacitor were constant. Later, Verbrugge and Liu[13] presented a one-dimensional electrochemical model with considering concentration profile applied to a single cell at an isothermal condition. However, these models were just

applied to a single cell, which cannot determine the temperature distribution in a whole supercapacitor. Meanwhile, the effect of temperature changes on the performance of the cell is neglected since constant physical properties were used.

On the other hand, due to the large scale of the supercapacitor stack, some thermal models often omit the electrochemical details of the individual cells. In reference[14-15], three-dimensional models were developed for a whole supercapacitor. In these models, the heat transfer equation with effective thermal conductivities for the core region, proper boundary conditions and homogenous constant heat generation rate fitted to the experimental data is considered.

In this study, a general multi-dimensional electrochemical-thermal coupled model has been developed for a supercapacitor. The electrochemical phenomena and thermal phenomena were treated simultaneously. To couple the 3D thermal model with 1D electrochemical model, temperature-dependent physical parameters, such as the electrolyte diffusion coefficient and ionic conductivity are used. The supercapacitor's temperature is calculated by the thermal energy balance equation. Then, the average temperature of the core region is fed back to 1D electrochemical model to update the electrochemical calculations by temperature-dependent physical parameters. Finally, the heat generation due to ohmic losses from the cell is returned to the energy equation to update the temperature. When coupled in this way, the thermal-electrochemical model obtained not only the supercapacitor cell behaviors, such as cell potential change, concentration distribution, heat generation rate and interfacial current density at any time during discharge and charge, but the thermal behaviors of the whole supercapacitor.

2 Mathematical modeling

The multi-dimensional electrochemical-thermal model was developed by coupling a 3D thermal model with a 1D electrochemical model where a spatially uniform but temporally varying heat source term is assumed. And the model structure is shown in Fig. 1.

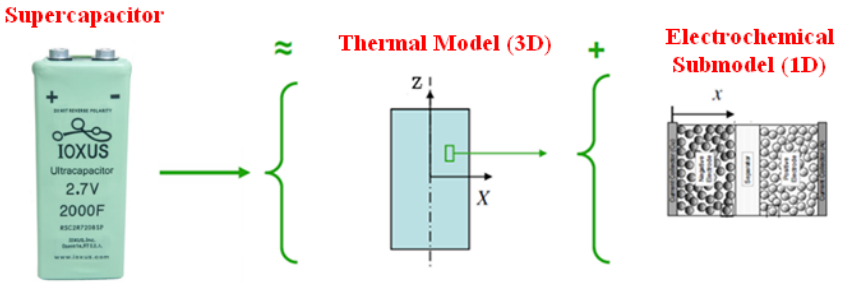

Fig. 1 Coupled electrochemical-thermal model structure

2.1 1D Electrochemical model

The external appearance of the Ioxus 2.7V/2000F supercapacitor is shown in Fig.1. It has five portions, namely, the core region, the gas region, the metal case, the terminals and the contact

layer. The core region consists of individual cells that are connected in parallel. The case is the container of the supercapacitor. The contact layer stands for a narrow gap between the core region and the case, which is generally filled with liquid electrolyte. There is a small volume of gas above the core region and underneath the top cover, where two terminals and a vent are installed. Since the electrochemical phenomena just happen in the core region, which includes individual cells connected in parallel, a single cell is needed for electrochemical analysis.

A typical supercapacitor cell consists of a negative electrode, an electrolyte separator, a positive electrode and two current collector, as shown in Figure 2. For a single cell, except both current collectors' top surfaces, other surfaces are treated as electrochemical insulation, meanwhile, current collectors have very large electrical conductivity compared with electrode and electrolyte, which means the current density at the interface between current collector and electrode can be assumed uniform. So, the electrochemical model can be simplified as a one-dimensional model, and it is similar to the one of Verbrugge et al[13]. Of course, the electrochemical model can be extended to a two-dimensional model, but the solution in conjunction with the thermal model for a full supercapacitor stack requires an excessive amount of computer memory and time and may not be practical.

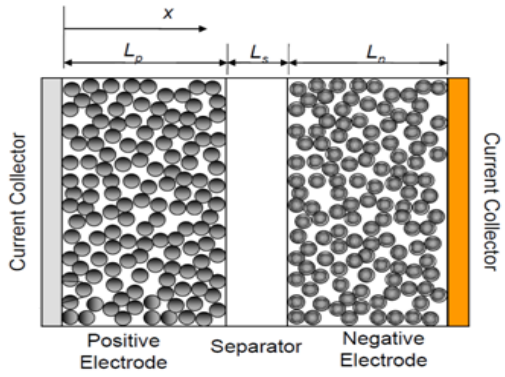

Fig. 2 Schematic of a single supercapacitor cell

Assumptions.--The electrochemical model used here assumes that the concentration, current, and overpotential distribution are one dimensional, only varying in the X direction. Temperature within each cell is uniform. This one is reasonable considering that each cell has a large effective thermal conductivity in the Y and Z directions (50 times larger than the effective thermal conductivity in the X direction) and the dimension in the X direction is small (the thickness of the cell is around 250μm, and the height and width of the cell are both of the order of 10cm).

So, the assumptions made in developing the model are summarized as : 1) Porous electrode theory in 1D is applicable; 2) all faradic reactions are neglected, and the energy storage mechanism is completely due to the charging of the double layer; 3)the electrolyte concentration gradient is considered; 4) ohmic losses are the dominating heating effect; 5) the double layer capacitance (Cdl) is a constant; 6) the diffusion coefficient and ionic conductivity of the

electrolyte's are functions of temperature and concentration, and other material properties are assumed to be constants; 7) the open circuit potential is set to zero, which means no self-discharge.

Governing equations.--The governing equations for the supercapacitor closely follow those of Verbrugge et al[13]. The material balance for the binary electrolyte gives rise to the conservation equation as

$$\varepsilon \frac{\partial c}{\partial t} = D_{eff} \frac{\partial^2 c}{\partial x^2} - \frac{\alpha C_{dl}}{F}\left(t_+ \frac{dq_-}{dq} - t_- \frac{dq_+}{dq}\right)\frac{\partial(\phi_1 - \phi_2)}{\partial t} \tag{1}$$

Note that q is charge density on the double layer surface. $\frac{dq_+}{dq} = 0$, $\frac{dq_-}{dq} = 1$ for an anion adsorbing (positive) electrode, and $\frac{dq_+}{dq} = 1$, $\frac{dq_-}{dq} = 0$ for a cation adsorbing (negative) electrode. $t_\pm$ is the transference number of the cation/anion. Depending on the combination of electrolyte and solvent, it can be a function of the electrolyte concentration. In present work, a constant value of transference number of electrolyte ion is assumed. Meanwhile, there is $t_+ + t_- = 1$.

The current densities in the solid matrix i_1 and the solution phase i_2 are given by

$$i_1 = -\sigma_{eff} \frac{\partial \phi_1}{\partial x} \tag{2}$$

$$i_2 = -\kappa_{eff}\left(\frac{\partial \phi_2}{\partial x} - \frac{2RT}{F}(1 - t_+)\nabla \ln c\right) \tag{3}$$

For an ideal solution, the relationship between the divergence of the current flow and the reaction rate in the capacitor is expressed as

$$\frac{\partial i_2}{\partial x} = \alpha C_{dl} \frac{\partial(\phi_1 - \phi_2)}{\partial t} \tag{4}$$

And the conservation of charge leads to the following equation

$$i_1 + i_2 = I_{app} \tag{5}$$

Here, I_{app} is the applied current density.

Electrochemical parameters used in the model are summarized in Table 1.

Table 1. Electrochemical parameters used in the simulation

Parameters	Value	Description
α (m^2/m^3)	$3x10^8$	Electrode surface area per unit volume of electrode
C_{dl} (F/m^2)	0.3	Capacitance per interfacial area
δ (S/m)	100	solid phase conductivity
$\varepsilon_{electrode}$	0.25	Porosity of electrode
ε_{sep}	0.7	Porosity of separator
c_0 (mol/m^3)	1000	Initial electrolyte concentration
Far (C/mol)	96487	Faraday's constant
Rg (J/K mol)	8.314	Gas constant
t_+	0.5	Cationic transference number

Porous electrode theory is applied in modeling the composite electrodes consisting of activated carbon and electrolyte. The solid and solution phases are treated as superimposed continua by considering the electrode porosity. Taking porosity into account, the electrolyte diffusion coefficient and ionic conductivity are evaluated by the Bruggeman relation, and given by the following expression:

$$\begin{cases} D_{eff} = D\varepsilon^{1.5} \\ \kappa_{eff} = \kappa\varepsilon^{1.5} \end{cases} \tag{6}$$

where ε is the electrode porosity. Similarly, the solid matrix conductivity is corrected as

$$\sigma_{eff} = \sigma(1-\varepsilon)^{1.5} \tag{7}$$

And the effective parameters in different sections of the supercapacitor cell are summarized in Table 2.

Table 2 Effective parameters calculation

Positive electrode	Separator	Negative electrode
$D_{eff} = D \cdot \varepsilon^{1.5}$	$D_{eff} = D \cdot \varepsilon^{1.5}$	$D_{eff} = D \cdot \varepsilon^{1.5}$
$\sigma_{eff} = \sigma \cdot (1-\varepsilon)^{1.5}$ $\kappa_{eff} = \kappa \cdot \varepsilon^{1.5}$	$\sigma_{eff} = 0$ $\kappa_{eff} = \kappa \cdot \varepsilon^{1.5}$	$\sigma_{eff} = \sigma \cdot (1-\varepsilon)^{1.5}$ $\kappa_{eff} = \kappa \cdot \varepsilon^{1.5}$

2.2 3D thermal model

The thermal model is a three-dimensional model as shown in Figure 3. It solves the heat transfer equation by a finite element method using commercial software COMSOL. Calculation of a three-dimensional temperature distribution within a supercapacitor made it easy to study different thermal management approaches

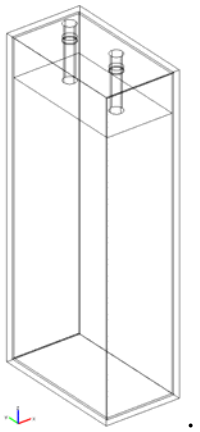

Fig. 3 the domain of the supercapacitor

The following assumptions are made to simplify the mathematical analysis of the problem. First, conduction is the main mechanism of heat transfer in the supercapacitor. This is because the liquid electrolytes are trapped in the porous structure of electrode and separator of the core region and the contact layer, the convective heat transfer in the core region can be neglected. Meanwhile, the supercapacitor system is opaque, the heat radiation inside a supercapacitor is not important; Second, in supercapacitor, heat generated due to ohmic and mass transport losses during charge/discharge processes is non-uniform distribution, considering the layered-structure of the cells. However, the thicknesses of each electrode, separator and current collector are very small compared with the whole dimensions of the core region, so the layered-structure of the core region can be treated as homogenous materials, and heat generation is uniform throughout the core region during charge/discharge processes; Third, since the core region is considered as homogeneous materials, the effective thermal conductivities of the core region can be estimated based on equivalent networks of parallel and series thermal resistances of the components[16].

With these assumptions, the transient 3D equation of heat conduction can be written as below:

$$\rho C_p \frac{\partial T}{\partial t} = \kappa_x \frac{\partial^2 T}{\partial x^2} + \kappa_y \frac{\partial^2 T}{\partial y^2} + \kappa_z \frac{\partial^2 T}{\partial z^2} + Q_{ohm} \tag{8}$$

For the core region, the product value of density and heat capacity is calculated based on the volume of each component as follows:

$$\rho C_p = \frac{\sum_i \rho_i C_{p,i} V_i}{\sum_i V_i} \tag{9}$$

The thermal model developed above requires knowledge of the local heat generation rate Q_{ohm}. This quantity can be calculated through the 1D electrochemical model. Since the heat generation is considered uniform for the whole supercapacitor stack core region, it is obtained by averaging the local heat generation rate over the cell thickness shown in equation (10).

$$Q_{ohm} = \frac{1}{L_{cell}} \int_0^{L_{cell}} (\sigma_{eff} \left(\frac{\partial \phi_1}{\partial x} \right)^2 + \kappa_{eff} \left(\frac{\partial \phi_2}{\partial x} \right)^2 + \frac{2\kappa_{eff} RT}{F} (1 - t_+) \frac{1}{c} \frac{\partial c}{\partial x} \frac{\partial \phi_2}{\partial x}) dx \tag{10}$$

And the detailed information on the supercapacitor and the simulation is summarized in Tables 3-4.

Table. 3 Thermal and physical properties of each material used in the simulation

Component	**Density** (kg / m^3)	**Heat capacity** ($J / kg \cdot K$)	**Thermal conductivity** ($W / m \cdot K$)	**Reference**
Metal case	2700	898.15	237	[17]
Activated carbon	700	700	5	[17]
Current collector	2700	898.15	237	[17]
Separator	930	1340	0.11	[17]
The contact layer	1352	263.5	0.6	[17]
Liquid electrolyte	779.3	2236	0.2	[17]
Gas	1.165	1006	0.026	[17]

At the boundary, both convection and radiation must be considered. For natural convection, the heat transfer coefficient can be determined as [17]:

$$h = f \left(\frac{T - T_\infty}{P} \right)^n \tag{11}$$

where, P is the characteristic length of the surface, and f and n are empirical coefficients. In comparison with constant heat transfer coefficient arbitrarily specified on the boundary as commonly used, this is closer to reality.

For forced convection, the heat transfer coefficient is weakly dependent on the local surface temperature, and can be treated as a constant value if the temperature variation is sufficiently small.

On the outside surface of the supercapacitor, besides convective heat transfer, the thermal energy can be transferred by radiation, which is propagated as a result of the temperature difference between a surface and its environment. The thermal radiation is proportional to the fourth power of the absolute temperature. The heat flux transferred is expressed as

$$q_{rad} = \varepsilon \cdot \sigma \cdot \left(T^4 - T_\infty^4\right) \tag{12}$$

where ε and σ are surface emissivity and Stefan-Boltzmann constant, respectively. In this paper, the radiation heat flux is written as the following relation:

$$q_{rad} = h_{rad}(T - T_\infty) \tag{13}$$

where the radiation heat transfer coefficient is expressed as

$$h_{rad} = \varepsilon \cdot \sigma \cdot \left(T + T_\infty\right)\left(T^2 + T_\infty^2\right) \tag{14}$$

Table. 4 Information of supercapacitor and setting of simulation

Dimension of supercapacitor	$6.4cm \times 3.6cm \times 15cm$
Dimension of unit cell	$6cm \times 0.023cm \times 12.8cm$
Dimension of core region	$6cm \times 3.2cm \times 12.8cm$
Thickness of the contact layer	$0.05cm$
Thickness of current collector	$0.001cm$
Thickness of electrode	$0.0075cm$
Thickness of separator	$0.004cm$
Thickness of metal case	$0.15cm$
Initial temperature	$298.15K$
Ambient temperature	$298.15K$

2.3 Numerical procedures

To couple the 3D thermal model with 1D electrochemical model, temperature-dependent physical parameters, such as the electrolyte diffusion coefficient and ionic conductivity are needed. In the present model, a total of five differential equations, Equations (1)-(4) and (8), are

solved simultaneously for the five unknowns: ϕ_1, ϕ_2, c, i_1, and T. A finite element method is used to solve these equations by commercial software COMSOL. The supercapacitor's temperature is calculated by the thermal energy balance equation. Then, the average temperature of the core region is fed back to update the electrochemical calculations by temperature-dependent physical parameters. Finally, the heat generation due to ohmic and mass transport losses from the 1D electrochemical model is returned to the energy equation to update the temperature. Thus, the electrochemical and thermal behaviors are coupled in this multi-dimensional model.

3. Results and discussion

3.1 Electrochemical behavior

The temperature and concentration dependencies of the properties of the electrolyte system used in this work (TEA-BF4 in PC) have not been reported in the literature. However, Valoen et al[19]. have reported the experimentally measured transport properties as functions of temperature and salt concentrations for LiPF6 in EC/DMC/PC. The correlations given by these authors were used here as approximations for estimating the performance of the system under thermal consideration.

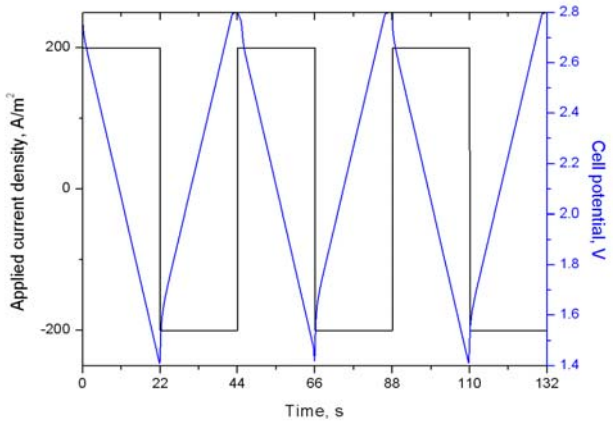

Fig. 3 Current and voltage versus time

Figure 3 represents the applied current density and the cell voltage variation according to the applied current, in which black curve shows the current density and the blue one is the voltage variation. The initial voltage and cut-off voltage of the cell are 2.8V and 1.4V, respectively, and the applied current density for discharge/charge is 200A/m^2.

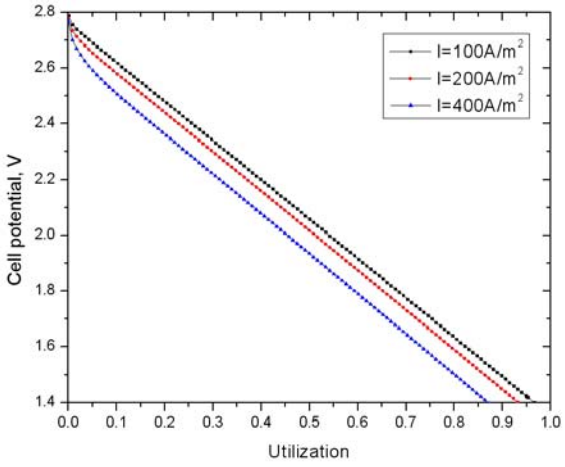

Fig. 4 Cell potential variation as a function of electrode utilization for different discharge rate

Figure 4 shows the cell voltage change as a function of utilization of positive electrode for several discharge rates from the initial voltage to cut-off voltage. The utilization of positive electrode is defined by equation 15, which represents the fraction of the available capacity extracted from the cell.

$$Uti = \frac{I_{app} \cdot t}{\alpha \cdot C_{dl} \cdot L_{electrode} \cdot (V_0 - V_{cut-off}) / 2} \tag{15}$$

Figure 4 is characterized by three features: (1) at the smaller current, the cell potential decreases linearly with time; (2) at the larger current, a sharp drop in voltage at the start of discharge is observed, which is followed by a linear decrease in potential for the rest of the discharge; (3) electrode utilization decreases as the discharge rate increases.

One primary consideration of supercapacitor design is how the electrode materials are utilized at different applied current densities. In Figure 4, we can find that electrode utilization decreases as increasing the discharge rate. At 100A/m^2 discharge rate, the cell utilization is about 96% at the end of discharge while the utilization deceases to 86% when the rate is 400A/m^2. This is because as discharge rate increasing, the steeper electrolyte concentration and cell potential gradient are created across the cell, and the ohmic effect becomes significant, which causes the capacity extracted from the cell when it reaches the cut-off voltage is less than the maximum capacity.

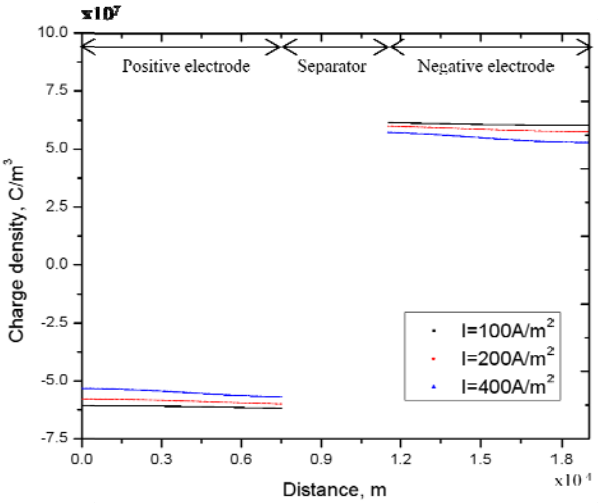

Fig. 5 Cell charge density profile at the end of discharge for different discharge rate

Corresponding to Figure 4, Figure 5 represents charge density profiles in the supercapacitor cell for different discharge rates when the potential drops to cut-off voltage. One can see at lower discharge rate the cell has a better uniformity in the charge distribution, which indicates a better electrode utilization. The trend is clear: higher discharge rates lead to non-uniform charge distribution and lower electrode utilization. Lower electrode utilization will result in additional cost, mass, and volume in designing supercapacitors.

3.2 Effect of porosity of electrode

The porosity, the electrolyte volume fraction in the electrode, has an important effect on supercapcitors in terms of overall capacity and utilization of the active material. We know if the porosity is high, the energy capacity of the supercapacitor is lower due to less active material into which electrolyte ions can intercalate to form the double-layer. However, if the porosity of the electrode is too low, electrolyte ions cannot effectively move through the liquid phase to the deeper regions of the electrode, and higher gradient in electrolyte concentration will be formed across the electrode as shown in figure 6, which will prohibit full utilization of the electrode. Meanwhile, from equation (10), we know higher concentration gradient will cause bigger heat source term and make the temperature of supercapacitor increase dramatically, which is demonstrated in Figure 7.

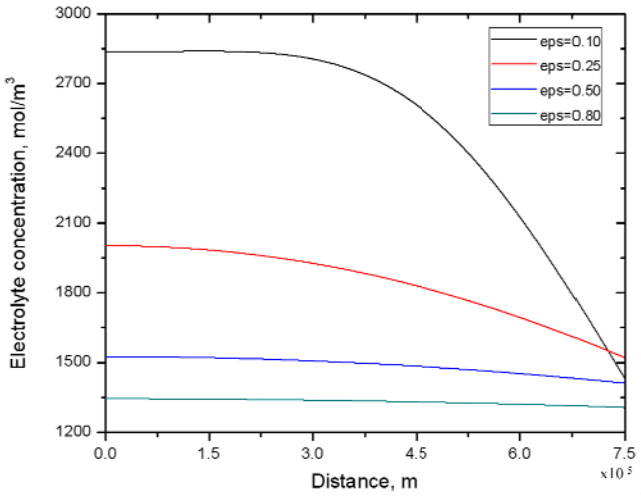

Fig. 6 Electrolyte concentration in positive electrode for different porosities at the end of discharge(the cell potential reaches the cut-off potential 1.4V) under 200A/m2 discharge rate

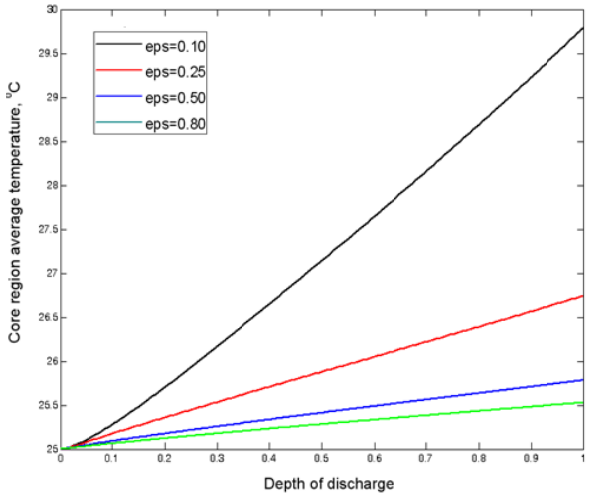

Fig. 7 Core region average temperature variation during discharge for different porosities under 200A/m2 discharge rate

3.3 Thermal behavior

The thermal behavior of a Ioxus company 2.7V/2000F type supercapacitor is examined in accordance with the multi-dimensional model proposed here. Information on the simulation is summarized in Tables 3 and 4. The effective thermal conductivity of the core region is better in the Y and Z directions ($23.6 W/m \cdot K$) than in X direction ($0.45 W/m \cdot K$). The natural convection and radiation is the default thermal condition at the boundaries, and the value of metal case emissivity is 0.25. The simulation is will be terminated when the maximum error in temperature is less than 10^{-6}K.

3.3.1 Temperature variation under galvanostatic discharge

The temporal evolution of the supercapacitor temperature during a discharge cycle under different discharge rates with natural convection and radiation is shown in Figure 8, which includes maximum, minimum and average temperatures of the supercapacitor. The average temperature is calculated based on components' volume as below

$$T_{average} = \frac{\sum_i V_i T_i}{\sum_i V_i} \tag{16}$$

In Figure 8, blue, red and black curves represent 400A/m^2, 200A/m^2 and 100A/m^2 discharge rates, respectively. We can find as the discharge rate increases, the maximum temperature increases and the temperature uniformity decreases significantly. This means thermal control is critically important when the supercapacitor undergoes high-rate discharge/charge cycle.

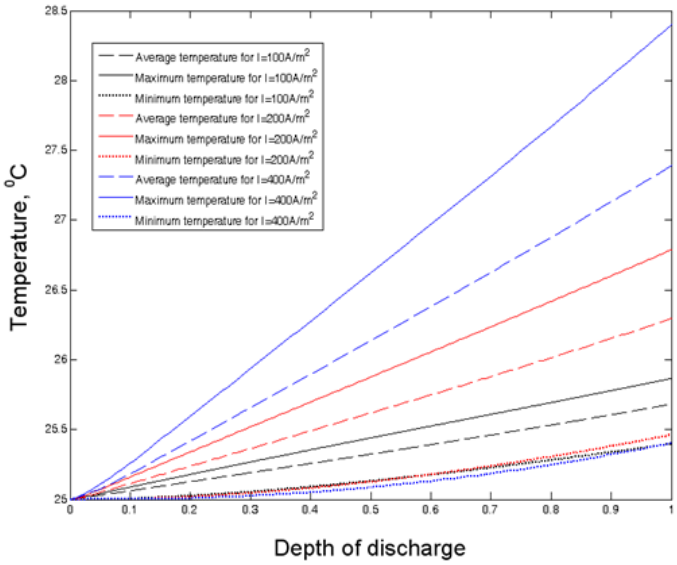

Fig. 8 Maximum, minimum and average temperature variation under different discharge rates

3.3.2 Temperature distribution within supercapacitor

The temperature distributions along X, Y and Z coordinates at the end of 10 successive cycles of 200A/m^2 are shown in Figure 9(a)-(c), respectively. The solid lines represent the temperature distribution along the centerline of the supercapacitor, and the dashed lines represent the temperature distribution on the surface. For solid lines, the temperature distribution in X direction is much steeper than that in Y and Z directions for core region. Due to poor conductivity of the contact layer and gas region and the excellent thermal conductivity of the metal case, these regions exhibit very steep and very gentle temperature gradients respectively. So, the temperature distribution across these components is easy to find. Both of dashed lines

have less sharp temperature gradient than the solid ones due to the good thermal conductivity of the case. According to Figure 9(a), the temperature on the surface (dashed lines) is lower than the temperature at the centerlines (solid line) in most of the region, but the opposite phenomenon can be found at the two sides. This is because the metallic container offers a shortcut for heat to flow from high temperature region to low temperature region. So a gentle temperature gradient is maintained on surfaces. However, the high thermal resistance in X direction of the core region depresses heat flow, whereby a steep temperature gradient is formed inside a supercapacitor. Therefore, such phenomenon occurs on both sides of the supercapacitor. Since the effective thermal conductivities in Y and Z directions of the core region are sufficiently large to prevent such temperature distribution, the phenomenon just occurs in X direction.

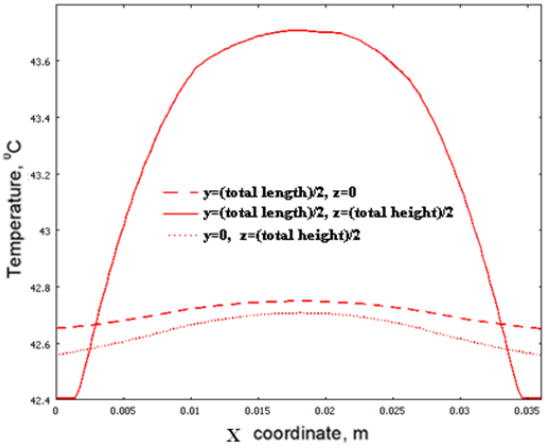

(a) Along X coordinate

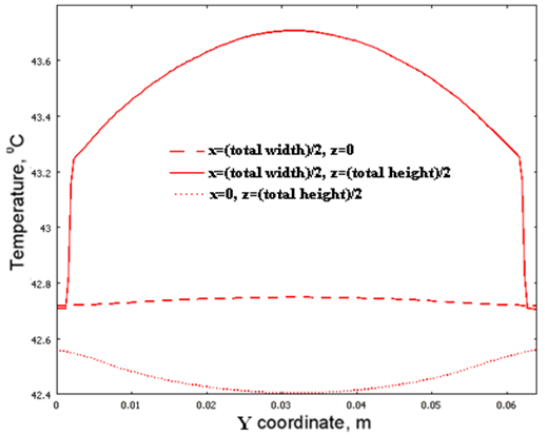

(b) Along Y coordinate

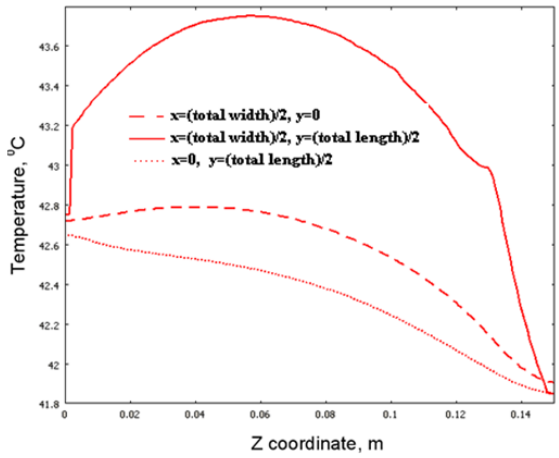

(c) Along Z coordinate

Fig. 9 Temperature distribution at the end of 10 cycles of 200A/m2 discharge/charge procedure

The contours of the temperature distribution on surfaces X=0 and Y=0 are shown in Figure 10 and Figure 11, respectively. The phenomenon discussed above become obvious. The results shown above indicates the effect of the contact layer is more significant in Y and Z directions than in X direction, because the effective thermal conductivity in X direction is poor (0.45) and is comparable with that of the contact layer (0.6).

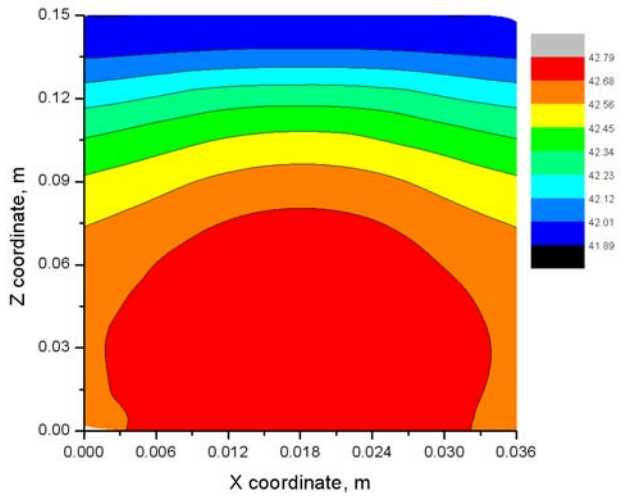

Fig. 10 Temperature distribution on the surface X=0 at the end of 10 cycles of 200A/m2 discharge/ charge procedure

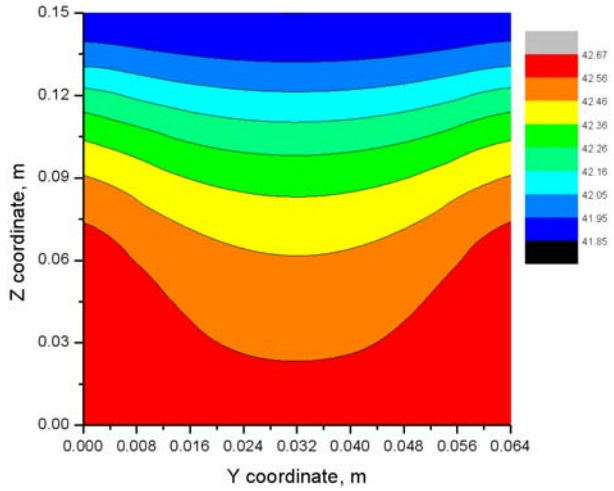

Fig. 11 Temperature distribution on the surface Y=0 at the end of 10 cycles of 200A/m2 discharge/ charge procedure

3.3.3 Heat dissipation mechanism on surface

The variation of natural convection and radiation heat transfer coefficients when the supercapacitor under 200A/m^2 discharge/charge rate is shown in Figure 12. The heat transfer coefficients are calculated based on the average temperature on each surface. The radiation heat transfer coefficients on all surfaces are very close to each other. The top surface (Z=0.15m) has the highest natural convective heat transfer, and the bottom (Z=0) gives the worst value. And at the end of 10 cycle of discharge/charge processes, the radiation heat transfer contributes about 25% for side walls, 33% for bottom wall, and 20% for top wall of the total heat transfer, respectively. This implies that radiation heat transfer cannot be neglected when supercapacitors are operated with natural convection.

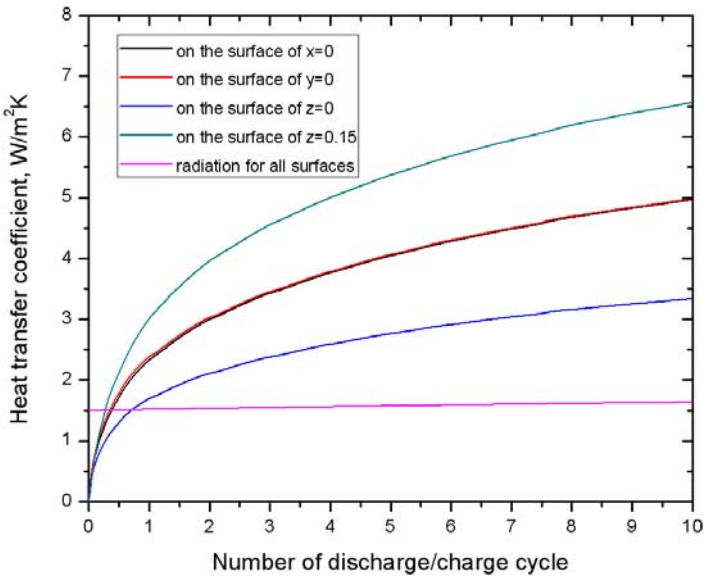

Fig. 12 Variation of convective and radiation heat transfer coefficient at 200A/m^2 discharge/charge rate with the emissivity is equal to 0.25.

3.3.4 Effect of forced convection

For the natural convection cooling, the maximum temperature of the supercapacitor will be higher than the maximum operating temperature when supercapacitors are subject to heavy duty cycling conditions. Therefore, force convection is employed whenever possible since it generally offers much better heat transfer than natural convection.

Figure 13 shows the evolution of the supercapacitor maximum temperature when it reaches steady state as a function of the convection heat transfer coefficient under 400A/m^2 discharge/charge rate. And the ambient temperature considered is 25^0C. These results show that the supercapacitor maximum temperature is higher than the maximum operating temperature when heat transfer coefficient is less than 32W/m^2K. In this condition, it is necessary to install a cooling system in order to maintain the supercapacitor temperature less than 65^0C.

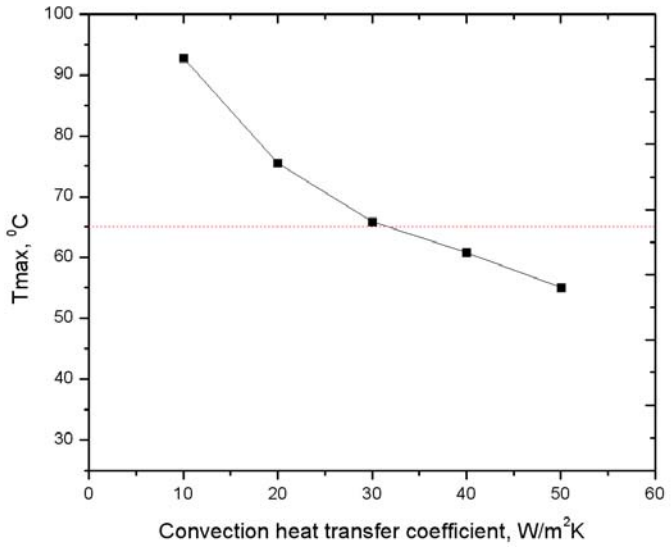

Fig. 13 Supercapacitor maximum temperature variation under 400A/m2 discharge/charge rate as a function of the convection heat transfer coefficient

A thermal management system is not only responsible for keeping the supercapacitor at an operating temperature, but also keeping the temperature distribution within the supercapacitor uniform.

Figure 14 (a) and (b) show the temperature distribution in X and Y directions for different cooling conditions at the end of 10 cycles of discharge/charge under 400A/m2 rate, in which the Y-axes represent the value of temperature minus the minimum temperature. By this way, we can clearly analyze different cooling methods how to affect the temperature gradient. In these figures, the black , red and blue curves represent temperature gradients under 50W/m^2K cooling applied for all surfaces, 100W/m^2K cooling applied for all surfaces, and 200w/m^2K cooling just

applied for Y direction surfaces, respectively, and the green curve shows the temperature gradient for 200W/m^{2}K cooling applied for Y direction and the contact layer's thermal conductivity increased from 0.6W/m·K to 15W/m·K.

Because the thermal resistance in X direction is very large, heat is difficult to remove from this way. Increasing the heat transfer coefficient in X direction simply increases the temperature gradient there as shown in Figure 14. However, because the effective thermal conductivity in Y direction is large, if the forced convective cooling just applied on the Y direction surfaces, the temperature distribution in the supercapacitor will be uniform.

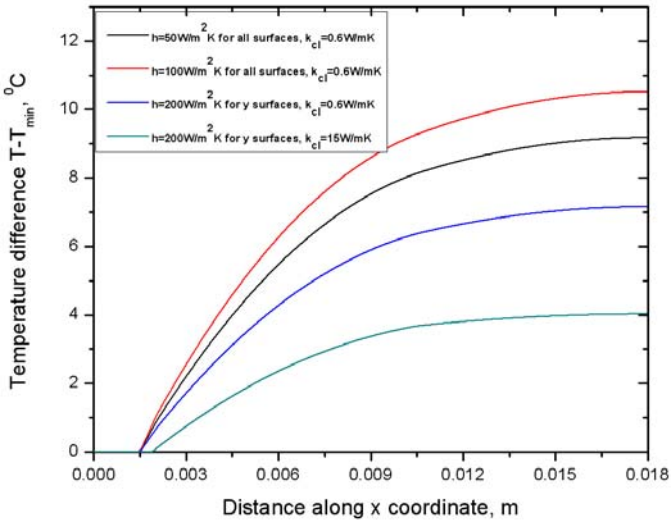

(a) temperature gradient along X direction

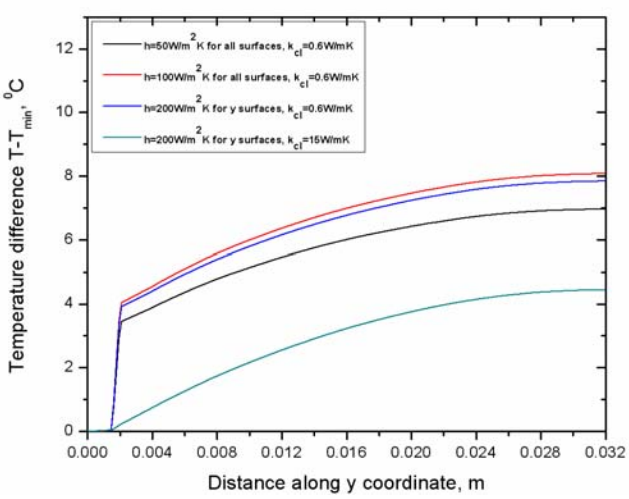

(b) temperature gradient along Y direction

Fig. 14 Temperature variation under different convection conditions at the end of 10 cycles of 400A/m2 discharge/charge

Finally, since the contact layer's thermal conductivity is poor (0.6W/mK), compared with Y direction core region's effective thermal conductivity(23.6W/mK), the contact layer acts like a thermal barrier. So, if increasing the conductivity of the contact layer, the temperature gradient in supercapacitor will become much more uniform as shown like green curve in Figure14.

According to the discussion above, the conditions of forced convection should be optimized to obtain a sufficient heat dissipation rate and acceptable temperature uniformity.

4. Conclusion

A coupled electrochemical and thermal multi-dimensional model is developed for studying the thermal management of supercapacitors and their electrochemical behavior. Detailed information, such as the electrolyte concentration, cell voltage, and heat generation rate in supercapacitor cells can be obtained. The electrochemical behavior of the supercapacitor cell under different discharge/charge rates and porosities in the electrode were examined. In thermal model, core region is simplified by adopting the average properties, and the contact layer and the metal case are all included. The thermal model considers the location-dependent convection and radiation heat transfer simultaneously to enhance the accuracy at the boundaries. Taking the simulation results, it can be seen that the maximum temperature increases and the temperature uniformity decreases significantly on increasing the discharge rate. A close look into the temperature distribution within the supercapacitor indicates that heat transfer is greater in Y and Z directions than in X direction, and the metal case and the contact layer are important components. Furthermore, radiation is found to be an important process for heat dissipation, especially in situations under natural convection. Applied strong forced convection on all surfaces is effective in depressing the maximum temperature inside the supercapacitor, but it decreases the uniformity and impairs the supercapacitor performance. Results from the simulation show if just applying forced convection on Y direction surfaces and increasing the contact layer thermal conductivity, the temperature gradient in supercapacitors will become more uniform, because of higher thermal conductivity in Y direction. Finally, the results obtained with this numerical model may be used to determine the cooling system required for actual supercapacitor applications.

B. Thermal Modeling of Clustered Cells

1. Introduction

In the earlier section, thermal analysis of a single supercapacitor was done by a multi-dimensional thermal and electrochemical coupled model. In this section, we will consider the supercapacitor module (supercapacitor group) as shown in figure 1. The supercapacitor used in the simulation is the Ioxus 2.7V/2000F one. The module studied in this paper is composed of 18 cells of 2000F, which are connected in series. The cells are arranged into six rows of three supercapacitors each.

Fig 1 structure of supercapacitor module

In order to study the thermal management of supercapacitor module, A steady-state fluid-thermal interaction CFD model in COMSOL was developed. The heat generated within the cells is transferred to an air flow maintained by natural or forced convection in the spacing between cells in the module. The thermal model assumes that heat transfer within the cells takes place by conduction only, and that heat transfer from module to the ambient air takes place by convection. The model makes use of two stationary application modes to simulate the problem: General Heat Transfer and Weakly Compressible Navier-Stokes.

Energy balance equation for each supercapacitor is

$$\nabla \cdot \left(-\kappa \nabla T \right) = Q - \rho C_p u \cdot \nabla T$$

since heat production in supercapacitors is related exclusively Joule losses, the heating power per unit volume is $Q = I^2 R_{esr} / V$, where I is the applied discharge/charge current, $R_{esr} = 0.45 \mu\Omega$ is the equivalent series resistance in DC state, and V is the core region volume. If the applied current is 100A, then Q is about 20000W/m^3.

2. Natural convection

Considering the symmetric property of the module' geometry, just one quarter of total geometry was chosen as the numerical domain as shown in Fig 2. In which, left and front boundaries are symmetry planes; right, back and top boundaries are open boundaries, respectively; and the bottom boundary is wall. Meanwhile, the ambient temperature is 25 degree C.

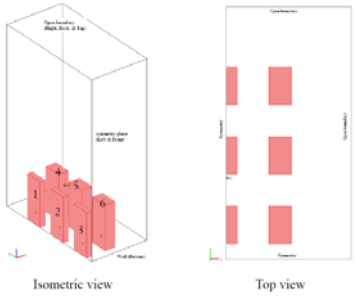

Fig. 2 Numerical domain and boundary conditions

The effect of air gap's width between supercpacitors on temperature was shown in Fig.3. This figure was characterized by three features: (1) at the start of increasing the air gap's width, the temperature would decrease sharply.(2) as air gap's width increasing, the temperature gradient decreases; (3) when the air gap's width is over 5cm , the maximum and minimum temperatures of the module gradually reach constant values. This is because when the air gap's width increases to a certain value, thermal boundaries of each single supercapacitor will not affect others', and the temperature distribution of every supercapacitor in this module becomes like the one of a single supercpacitor under natural convection.

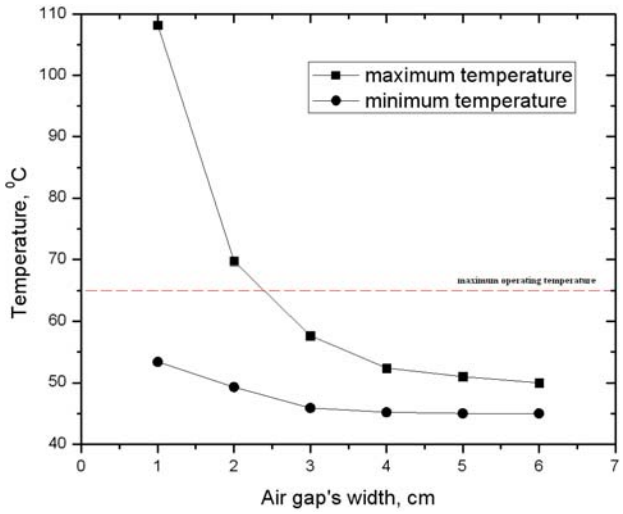

Fig. 3 Effect of air gap's width on the temperature at 100A applied current rate

For the natural convection cooling, the maximum temperature of the supercapacitor will be higher than the maximum operating temperature when the module is subject to heavy duty cycling conditions. Therefore, force convection is employed whenever possible since it generally offers much better heat transfer than natural convection.

3. Forced convection

There are three different forced convection cooling methods as shown in Fig. 4, which are air flowing from front boundary of the module, air flowing from left boundary of the module, and air flowing from top boundary of the module (impinging fan flow), respectively. And other conditions are: (1) the applied current is 100A, which leads to a 20000W/m3 heat source term for each cell; (2) inlet air velocity is 1m/s; (3) ambient temperature is 25 degree C.

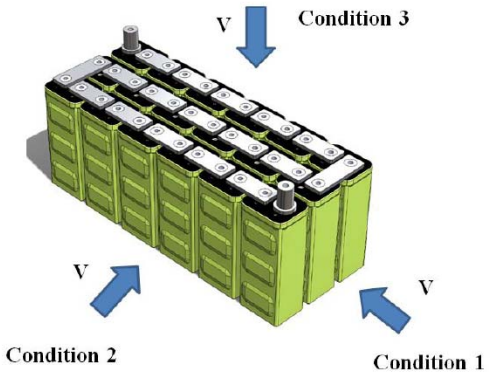

Fig. 4 Three different forced convection cooling methods

Considering the symmetric property of the module, in Fig. 5, only one part of the module was chosen as the numerical domain for these three cooling methods.

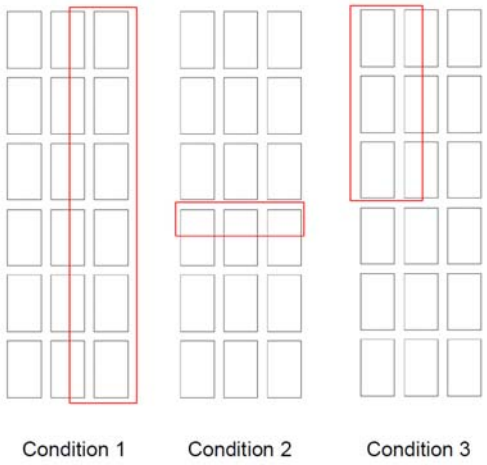

Fig. 5 Top view of module and the chosen numerical domains (regions in red rectangular curve)

Fig. 6 (a)-(c) shown the steady-state temperature results for three cooling methods. Fig. 6(a) is the module's temperature distribution for first cooling method. The maximum temperature (92 degree C) in the module is much higher than the maximum operating temperature (65 degree C).

Meanwhile, average temperature for each cell in the module was calculated based on components' volume as below

$$T_{average} = \frac{\sum_i T_i V_i}{\sum_i V_i}$$

The last cell in the first column has the maximum average temperature(87.4 degree C), and the first cell in the second column has the minimum average temperature (29.3 degree C). Fig. 6(b) is the result for second cooling method, in which the maximum temperature is 45.5 degree C. And the cell maximum average temperature is 44.1 degree C, and the cell minimum average temperature is 30.7 degree C. Finally, Fig. 6(c) shows temperature distribution for third cooling method. The maximum temperature is 42 degree C. And the cell maximum and minimum temperatures are 39 degree C and 33.6 degree C, respectively. All of these data are summarized in Table 1.

Compared with two other methods, using impinging forced convection cooling, the module has lower maximum temperature and uniform temperature distribution. So this method is the best one.

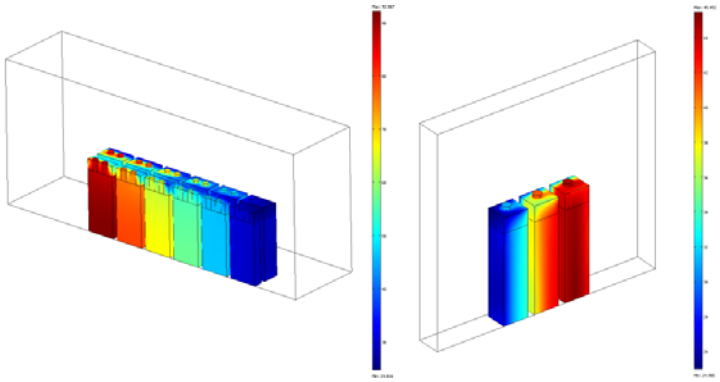

(a) Condition 1 (b) Condition 2

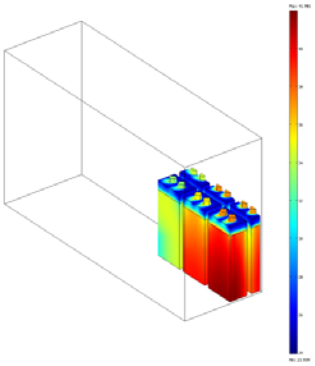

(c) Condition 3

Fig. 6 Module's temperature distribution for three different cooling methods

Table. 1 Numerical results for three cooling methods

	Maximum temperature of the module (degree C)	Average temperature of the module (degree C)	Maximum average temperature of single cell (degree C)	Minimum average temperature of single cell (degree C)
Method 1	92	60.6	87.4	29.3
Method 2	45.5	38.5	44.1	30.7
Method 3	42	36.6	39	33.6

Next, the optimization problem considered in this study is to maximize the thermal performance of the supercapacitor module with impinging forced convection cooling system. To capture the reverse flow at the exit of the module, we extend the computational domain to five times the module dimension in the x and y directions from the symmetric surface. Fig. 7 shows the detailed dimension of the module for one quarter of the full domain and boundary conditions. Cooling air is impinged normal to cell array, and then the air exits in the x and y directions through flow passages between the cells. So the top plane is velocity inlet boundary; left and back planes are pressure outlet boundaries; front and right planes are symmetries; and the bottom plane is adiabatic wall.

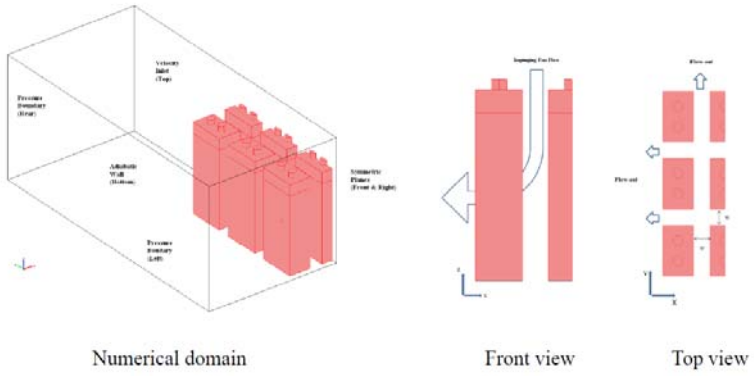

Fig. 7 Schematic of supercapacitor module with impinging fan flow cooling system

The optimization of air gap's width in the supercapacitor module is conducted numerically. The flow and thermal fields for the extended computational domain, including the module, are solved to determine the temperature distribution. Thereafter, the optimization of air gap's width can be obtained.

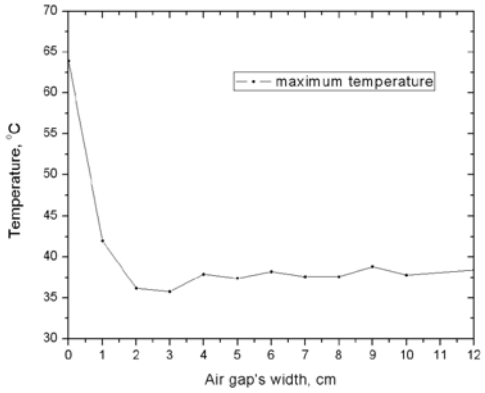

Fig. 8 Effect of air gap's width on the maximum temperature of the module at 100A applied current rate

The temperature for various air gap's widths is shown in Fig. 8. This figure shows that as the air gap's width increases, the maximum temperature decreases. And when the width is larger than 3cm, the temperature gradually reaches steady state. This is because as the width increasing, the velocity boundary and thermal boundary of each cell will not be affected by others, and the temperature distribution for each cell will not change.

4. Summary

Compared with other two kinds of forced convection cooling methods, the impinging forced convection cooling has the better results. Changing the air gap's width between supercapacitor cells can affect the velocity distribution, which further changes the heat transfer coefficient on the surfaces of supercapacitors. It can be found that at the start of increasing the air gap's width, the temperature would decrease dramatically. When the width is larger than 3cm, the maximum temperature reaches steady state. So, the optimization of the air gap's width is 3cm.

C. Materials Characterization and Formulation Optimization Study: Optimization study of electrode material composition to enhance supercapacitor performance

1. Introduction

Supercapacitors or the Electric double layer capacitors (EDLC's) have evoked wide interest in recent years due to their ability to supply high power in short-term pulse, which make them very good energy storage devices for applications such as hybrid power sources for electrical vehicles, portable electronic devices, uninterruptible power supply (UPS), and pulse laser techniques. For applications in which significant energy is needed in pulse form, traditional capacitors as used in electronic circuits cannot store enough energy in the volume and weight available. For these applications, the development of high energy density capacitors has been undertaken by various groups around the world.

Optimization of the electrode with increase in power and energy density along with lowering the cost is one of major needs. The electrode is the key part of the electrochemical capacitors (ECs), so the electrode materials are the most important factors to determine the properties of ECs. Activated carbon (AC) is the electrode material used most frequently for EDLCs due to the low cost, high surface area, availability, and established production technologies. In this report, we examined the structure and particle size distribution for various active carbons, and also looked into the optimization of electrode material composition, based on performance in terms of capacitance of the electrode.

The electrode basically consists of slurry of 2 different types of carbons and a binder solution coated onto collector. The two carbons considered for this study are the high surface area activated carbon (active carbon) and super P (conductive carbon). The active carbon is the basis of energy storage in the supercapacitors while the conductive carbons are additives for increase in electrical conductivity across the electrode surface. The mixing of the two carbons is also an important aspect for efficient performance of electrode. Earlier studies were done on different types of electrode materials like carbon nano- tube and their performance. The materials used in this study were characterized for their surface structures, surface area, and particle size distribution.

A prototype of electrode was constructed to evaluate the optimization of composition of materials. The electrode behavior and thus its performance were analyzed in terms of capacitance values obtained from running the electrode in a test cell setup.

A schematic of a supercapacitor is shown in Fig. 1. The ions displaced in forming the double-layers in the pores are transferred between the electrodes by diffusion through the electrolyte.

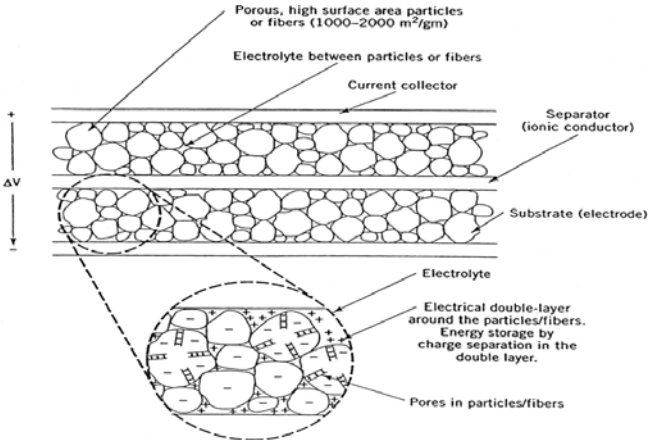

Figure 1. A schematic diagram for cross section of an electrode

The capacitance is dependent primarily on the characteristics of the electrode material surface area and pore size distribution. In this study we will primarily focus on the material characterization of the electrode material. Active carbon is used as one of the constituent material for the preparation of electrode as it has a very high specific surface area. But at the same time it also reduces to conductivity through the electrode. To increase the electrical conductivity conductive carbons are mixed with activated carbons. A potentiostat was used to analyze the behavior of the electrode in terms of its capacitance and series equivalent resistance (ESR).

2. Experimental Procedures

2.1. Characterization of active and conductive carbon materials

Five active carbons from various sources were characterized. Out of the 5, the active carbon showing highest surface area was selected for the actual experimentation. Conductive carbon provided by Ioxus (Super P) was used to fabricate electrodes for experiments.

2.1.1. Scanning electron microscopic observation

Particle shape and size distribution was examined using SEM. Images taken for the five active carbon samples are shown below in Fig. 2a – 2e.

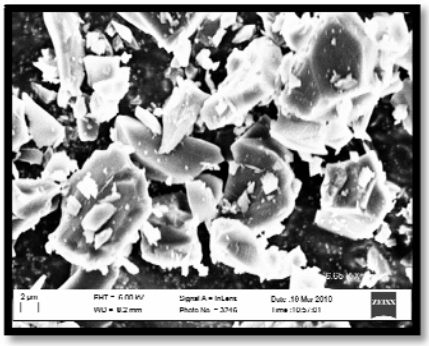

a

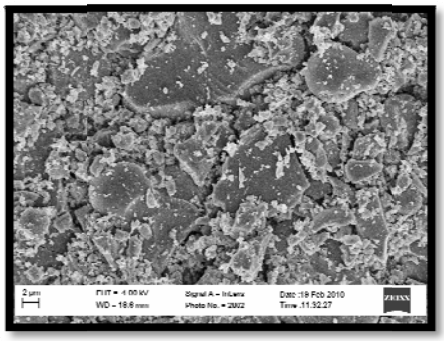

b

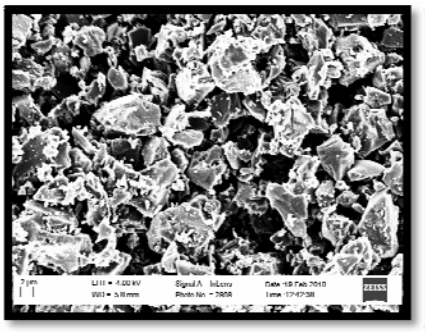

c

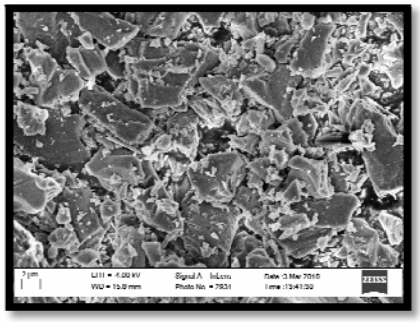

d

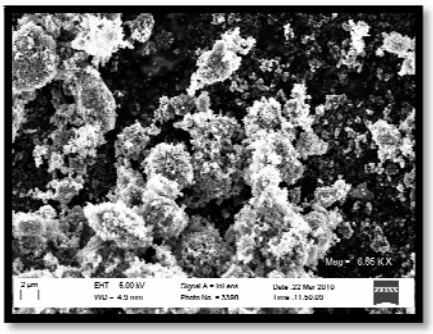

e

Figure 2. SEM Images of various active carbon powders. Powder samples were provided by Ioxus, and designated as a through e. Active carbon a (MSP 20) is the one used by Ioxus for manufacturing.

Estimated particle size of various active carbons are tabulated below

Table 1. Large particle size estimated from SEM images

Active carbon	Particle size range (microns)
a	5 - 10
b	8 - 12
c	9 - 11
d	3 - 16
e	Aggregation of nano size particles

An SEM image of conductive carbon is shown in Fig.3.

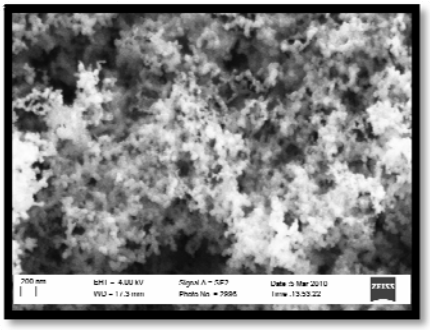

Figure 3. SEM image of conductive carbon

Particle size of conductive carbon is much smaller than that of active carbon. It is in the order of several nano meters in diameter.

2.1.2. Quantitative analysis of particle size

The particle size distribution was analyzed using an instrument manufactured by Beckman & Coulter (LS13320 model)

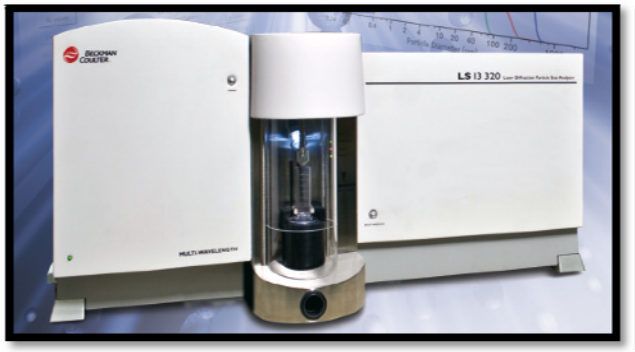

Figure 4. LS13 320 with Tornado dry powder module attached.

Powder samples were ultrasonicated prior to analysis to break up aggregated particles. Plots for volume % vs particle diameter are shown in Fig. 5a – Fig. 5d. Since minimum measureable particle size is 4 microns for LS13320 system, we did not attempt to analyze particle size distribution of powder sample e and conductive carbon.

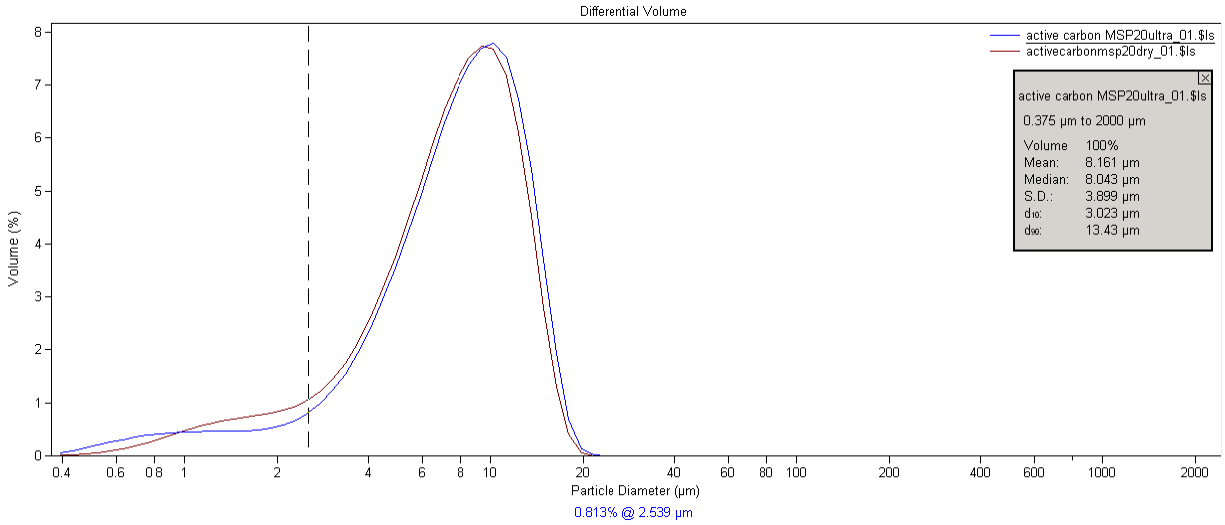

Figure 5a Volume % vs. particle diameter of sample a (MSP 20)

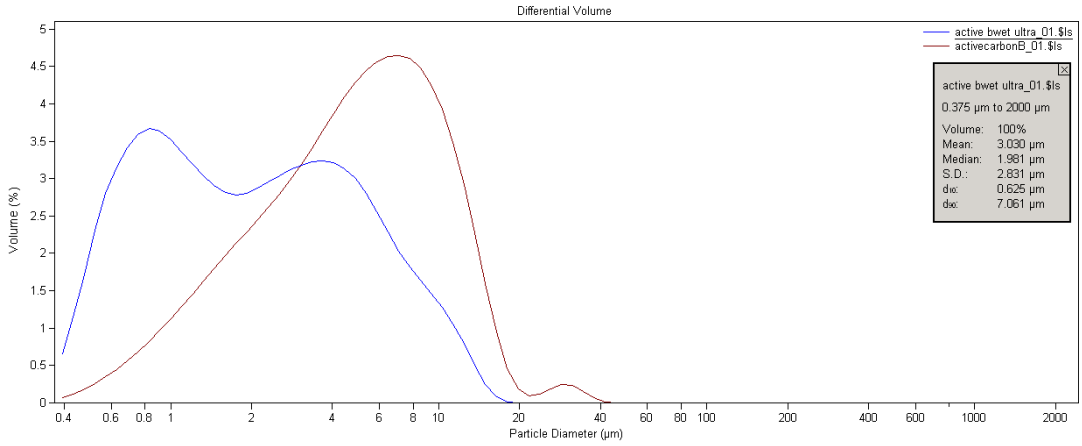

Figure 5b Volume % vs. particle diameter of active carbon b

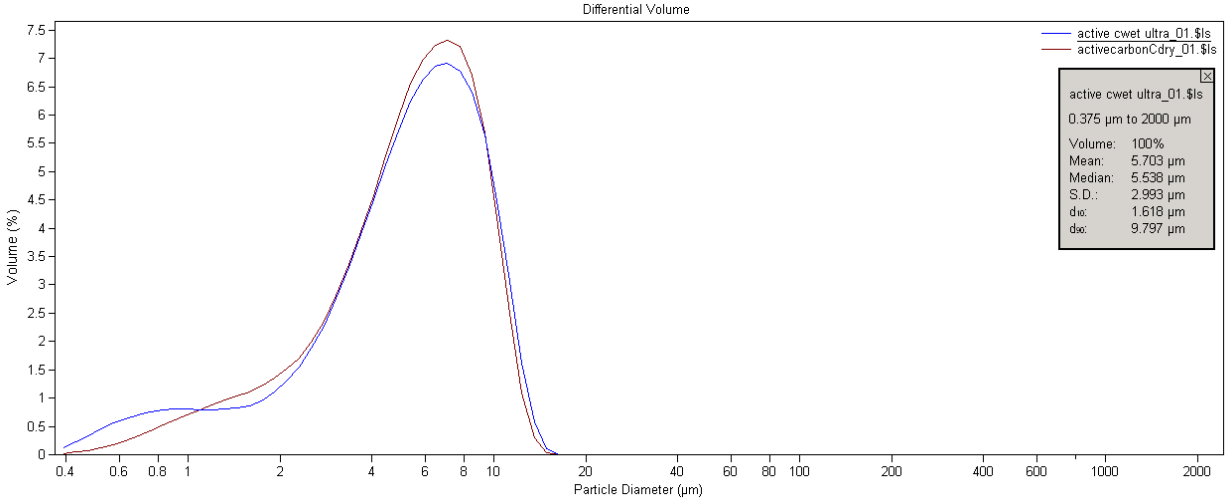

Figure 5c Volume % vs. particle diameter of active carbon c

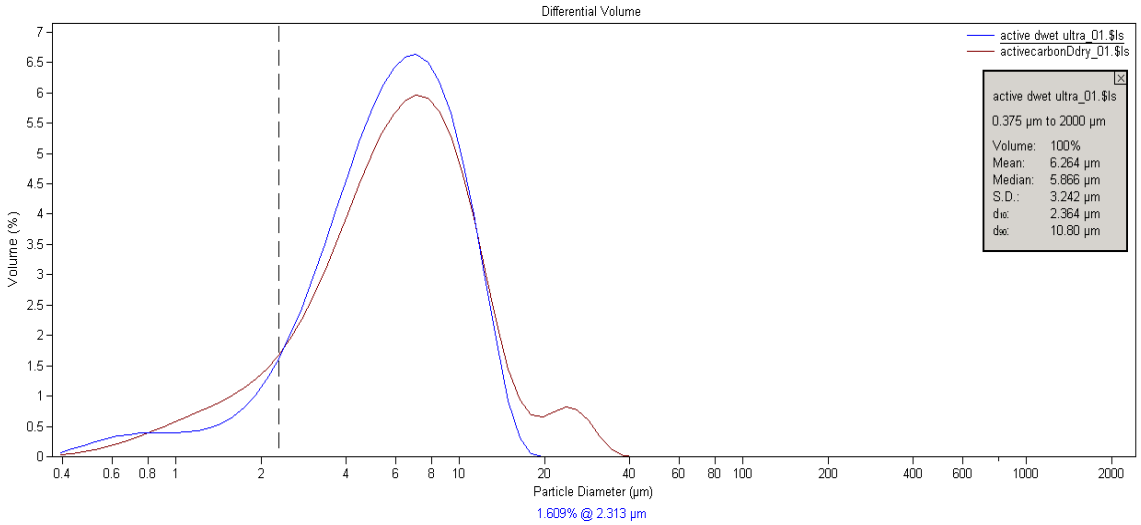

Figure 5d Volume % vs. particle diameter of active carbon d

As shown in Figure 5, active carbon a (MSP 20) has size ranging from 0.4 to 20 microns. With maximum volume percentage involved particles having size ranging from 6-15 microns. A summary of the particle size distribution is shown in Table 2.

Table 2. Particle size range and maximum volume % size range

Active carbon	Particle size range (microns)	Maximum volume % range (microns)
a	0.4 - 20	6 - 15
b	0.4 – 20	6 - 15
c	0.4 - 15	6 - 10
d	0.4 – 20	6 - 15

Large particle size estimated from SEM images shown in Table 1 is somewhat different from the result summarized in Table 2. It is believed that the difference is attributable to sampling and limited view of SEM observation. While powder c shows a little smaller particle size than a, b, and d which showed the same particle size distribution.

2.1.3. Surface Area Analysis of Active and Conductive Carbons

Surface area measurements were made a Beckman oulter SA 3100 Surface analyzer system. The SA 3100 is a bench top BET surface area and pore size analyzer, which uses the static dosing method. This reference method uses helium to measure the sample tube free-space for highly accurate data.

Figure 6. SA3100 Surface analyzer

A summary of surface area measurements for various active carbon powders is shown in Table 3.

Table 3. Measured surface area values for various active carbon powders

Active carbon sample	Surface area (square meter /gram)
a	2150.28
b	1759.70
c	1549.55
d	1296.85
e	57.62

While powder e has the smallest particle size as shown in SEM images, it has the lowest effective surface area. Among the 5 active carbons tested powder a (MSP 20) has the highest surface area.

This characterization showed that the active carbon has a very large surface area which is important in terms of capacitance of the supercapacitor. The particle analysis showed that the active carbons MSP 20 have particle size in the range of 6 - 15 microns while conductive carbons (Super P) are very fine particles having size in few nanometers. It is believed that conductive carbon would serve the purpose of increasing the conductivity as its fineness provides a better electrical contact between active carbons by filling gabs between large active carbon particles.

2.2. Electrode sample preparation

The electrode is the key part of the electrochemical capacitors (ECs), so the electrode materials are the most important factors to determine the properties of ECs. Samples of specimen electrode were prepared to test for capacitance and ESR .

2.2.1. Electrode preparation

The preparation of the specimen electrode involved a number of processes which are explained as we proceed. The schematic of the process is given as follows

a. Mixing of dry carbons (Active Carbons and Conductive Carbons)
b. Binder solution preparation
c. Mixing of dry carbon mixture and binder solution (slurry preparation)
d. Coating of slurry onto Aluminum Foil
e. Drying the electrode (Oven drying)

For each process step different instruments were used will be described in the process description given below which are discussed below:

a. Mixing of dry carbons
This is the initial step of the electrode preparation process. The conductive carbon and active carbons of required quantity are mixed together till they form a homogeneous mixture. This is done by mixing them in a planetary mixer for a specified period of time. The planetary mixer used in our study is Kurabo Mazerustar which is as shown below.

Figure 7. Kurabo Mazerustar

b. Binder Solution Preparation
Binder solution preparation is the next step that is undertaken .It involved preparation of the adhesive solution from following materials:

- CMC
- PTFE (emulsion)
- Florosurfactant

CMC and PTFE emulsion are major constituents of binder while, the flourosurfactant is an additive which helps in increasing the conductivity of the electrode though conductive carbon percentage is reduced. The binder solution is prepared by mixing these materials with water in a beaker with the help of magnetic stirrer. The solution preparation time is approximately 50 minutes. The picture shows binder solution being prepared in a beaker.

c. Electrode slurry Preparation

The electrode slurry is prepared by mixing the binder solution prepared and the dry carbon mixture. The mixing time is 50 minutes and the instrument used is Kurbo Mazerustar, the same instrument used for the dry mixing of the electrodes.

d. Electrode coating

Electrode coating is the process which involves coating of the electrode slurry onto the current collector surface .The collector that has been used for this study is aluminum foil having thickness of 20 microns. The electrode coating is done with the help of the instrument Automatic film applicator **(**MTI Corporation EQ-AFA-I automatic coater**)** that is shown in the figure below.

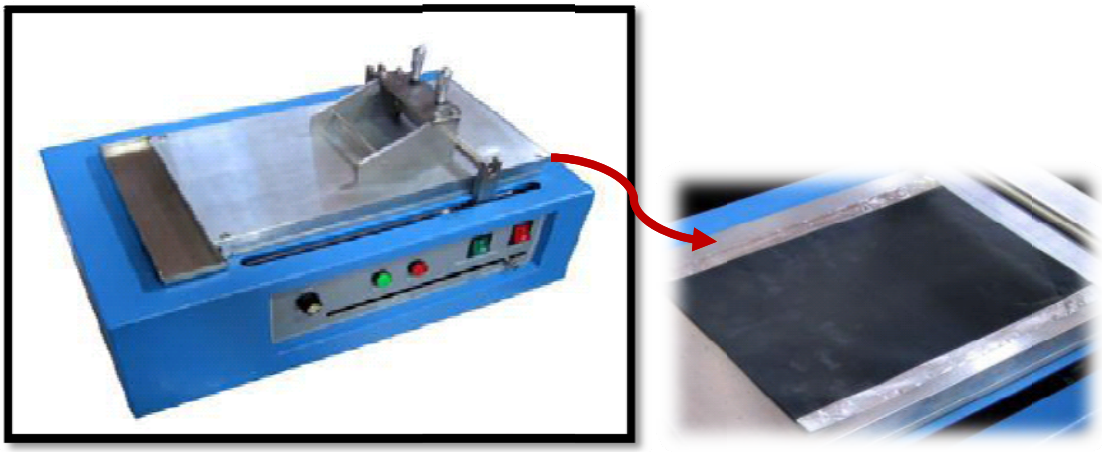

Figure 8. MTI Corporation EQ-AFA-I automatic coater

It consists of variable thickness doctor blade which moves over vacuum bed as shown in the figure. With the help of variable thickness doctor blade electrode with desired thickness ranging from can be obtained. The next step that is involved in the task of electrode preparation is the drying process.

e. Electrode Drying

This process is carried out by using the oven. The coated electrode was placed onto a flat metal plate and dried for 1hour at 75^{o}C. The picture shows the binder oven used for the drying process.

Figure 9. Oven used for drying

The time required for drying the electrode was established on the basis of thermo-gravimetric analysis (TGA) of the electrode slurry as shown in the following figures.

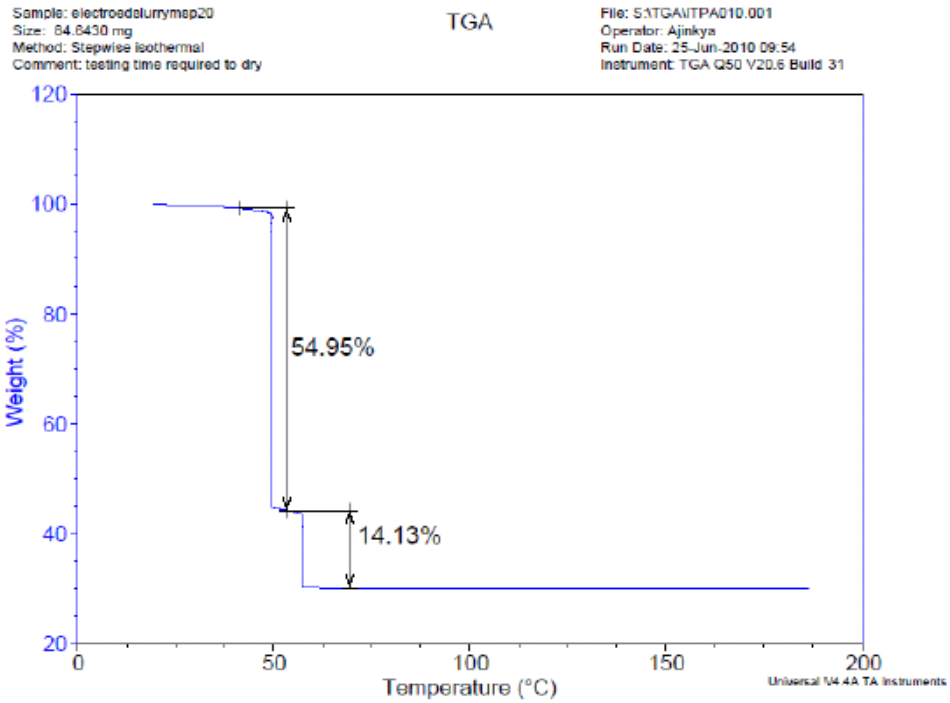

Figure 11. Weight loss in percentage vs. temperature

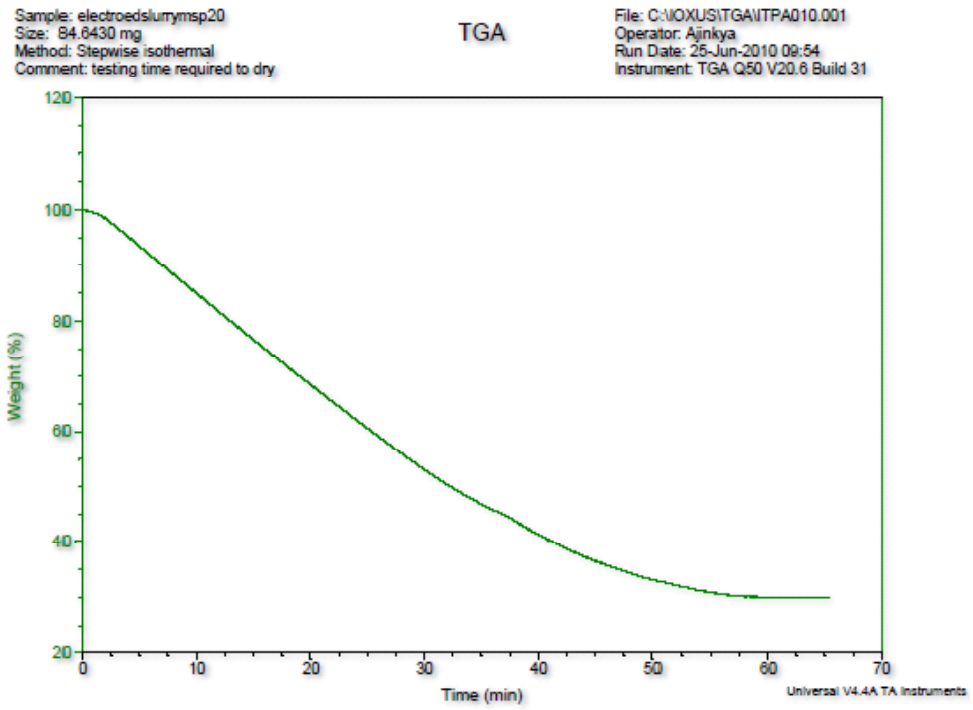

Figure 12. Weight loss in percentage vs. time in minutes

As shown in the TGA result, powder a (MSP20) and conductive carbon (Super P) slurry became completely dry when it was heated up to 60^0C for approximately 50 minutes. Sample electrodes were dried at 75^oC for an hour to make sure that the electrode had dried off completely. After the drying of the electrode, the next step is sample preparation. Electrode samples are prepared for testing by cutting into coupons of size 20mm X 20mm.

2.3 Active carbon, conductive carbon, and binder compositions

After the initial material characterization of the materials selected for specimen preparation the next step was test cell setup. The samples for the tests were prepared with procedure as discussed earlier. Electrodes with different compositions (varying percentage by weight of conductive carbons) were prepared to find an optimum composition for electrode. Electrodes with various compositions were prepared according the following Table compositions

Table 4. Electrode compositions

Active carbons (wt %)	Conductive carbons(wt %)	Binder (wt %)
87	5	8
85	7	8
82	10	8
77	15	8

The total weight considering carbons and binder solution neglecting the amount of water was considered 20gm. The dry mixing time and the mixing of binder solution and the dry mixture to form electrode slurry were taken to be 50 min for each of the processes. The aluminum foil was coated on the single side on automatic film applicator. The drying process of coated electrode was carried out in an oven for 60 min the temperature being kept 75^o C. The thickness of electrode was kept to be 100 microns for all compositions. Electrode coupons were prepared for the purpose of testing. The electrodes thus prepared will be tested with the help of beaker cell arrangement for the purpose of measurement of capacitance. Further on various parameters the behavior of the electrodes prepared will be tested to find out the optimum composition and the next step would be optimization of thickness of electrode.

2.4. Electrode test cell setup

2.4.1. Electrode testing setup

The prepared test cell was tested at IOXUS with the help of instrument Potentiostat HCP-803(BioLogic) available there. Multiple tests were undertaken to get consistent results.

Electrodes were tested using a potentiostat. The electrochemical test cell was charged to a certain voltage at specified current and was held for specific period of time. Later it was discharged. The charge discharge characteristics were analyzed to calculate the capacitance and the ESR of the electrode specimen.

The Calculations were carried out by following formulae

Capacitance = I*(tf-t1)/ (V1-Vf)

where I = Current V1 = Initial voltage Vf = final voltage

V2= voltage after sudden downsurge of voltage.

ESR = (V1-V2)/I

3. Results and Discussion

The initial tests were run to confirm whether the test equipment setup has a proper functioning or not. The coupon electrode of size 1.5 X 1.5 cm was tested on the potentiostat and the capacitance obtained for the electrode was 0.9 Farads. The next step was actual behavior study with change in composition of active and conductive carbons. The single sided electrode was tested for following compositions. The electrode thickness was kept 100 microns, excluding the thickness of the electrode. The charge/discharge characteristics were obtained by following the process of charging the electrode to 1.5 volts holding it for 10 min and then following the discharge. These characteristics helped in finding the capacitance and the ESR of the specimen electrode tested. Five samples of each electrode composition were tested. To minimize inaccuracy of capacitance value due to slight variation in nominal area of coated carbon coupon it was normalized with nominal area of 1 cm^2. A summarized capacitance and ESR data are tabulated in Tables 5 and 6.

3.1. Capacitance data

Electrode number	Conductive carbon percentage 5% Capacitance in Farads/sq.cm	Conductive carbon percentage 7% Capacitance in Farads/sq.cm	Conductive carbon percentage 10% Capacitance in Farads/sq.cm	Conductive carbon percentage 15% Capacitance in Farads/sq.cm
1	0.6915	0.54501	0.8175	0.634
2	0.652019	0.5894	0.697427	0.6708
3	0.619	0.7048	0.62	0.6738
4	0.6237	0.7173	0.6747	0.6015
5	0.59	.60515	.6224	0.66850
Average	0.635244	0.63135	.6864	0.6497
Std. Deviation	+/-0.03809	+/-0.083114	+/-.214	+/-.0245

3.2. ESR data

Electrode number	Conductive carbon percentage 5% ESR in Ohms/sq.cm	Conductive carbon percentage 7% ESR in Ohms/sq.cm	Conductive carbon percentage 10% ESR in Ohms/sq.cm	Conductive carbon percentage 15% ESR in Ohms/sq.cm
1	8.96	8.184	6.573	8.364
2	9.50	8.737	8.300	7.066
3	10.34	10.075	8.476	7.387
4	8.49	6.849	7.29	6.973
5	12.514	7.20	8.20	7.79
Average	9.9608	8.209	7.768	7.5152

The results show that there is lack of consistency in the values of capacitance and ESR in most of the compositions. The factors for these irregularities can be various such as damage of electrode, thickness limitation, insufficient mixing etc. Also, the behavior can't be predicted from the trend line observed in the graph as there is not much change in the values and they aren't consistent.

Literature study suggested that the electrode preparation time should be well sufficient for mixing of the carbons. So, the mixing time was increased to 50 minutes earlier which was 15 minutes. The size was increased to 2cmx2cm to minimize the irregularities in the values.

Electrodes were tested for capacitance with increment in current in a single run. Data was analyzed and the linearity of the curve was studied. The capacitance value obtained was normalized with Farads / gm of carbon coating to further minimize the electrode irregularities as discussed earlier. The results show that linearity is seen when current increases beyond 12 mA and a distinct behavior is seen in terms of capacitance values for different compositions with increase in current .So, it was concluded from these results that a current more than 12 mA was required to get a distinct behavior of the electrode performance in terms of capacitance.

Further tests were undertaken for electrodes prepared with the 4 compositions with the mixing time increased upto 50 min and electrode size kept 2cm X 2cm.The current value was set at 20 mA. The charge discharge characteristics were observed and analyzed as shown below.

3.3 Further capacitance data

Electrode number	Conductive carbon percentage 5% Capacitance in Farads/gm	Conductive carbon percentage 7% Capacitance in Farads/gm	Conductive carbon percentage 10% Capacitance in Farads/gm	Conductive carbon percentage 15% Capacitance in Farads/gm
1	92.197	118.141	111.184	93.77
2	102.168	114.271	107.847	99.893
3	96.261	130.513	115.773	91.807
4	122.631	121.217	106.515	97.674
Average	96.8753	117.876	110.33	95.786
Std. Deviation	5.01381	8.48377	4.12614	3.66646

Figure(21) shows :Typical charge discharge curve

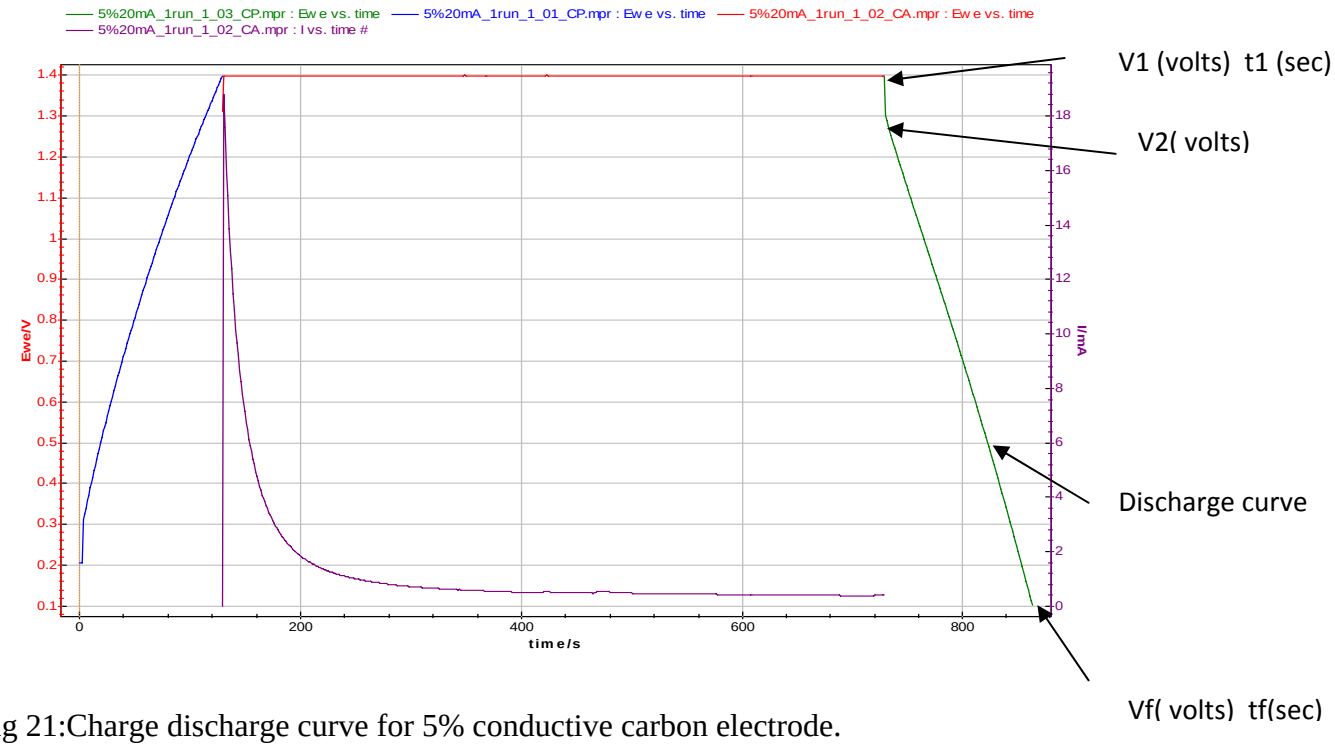

Fig 21:Charge discharge curve for 5% conductive carbon electrode.

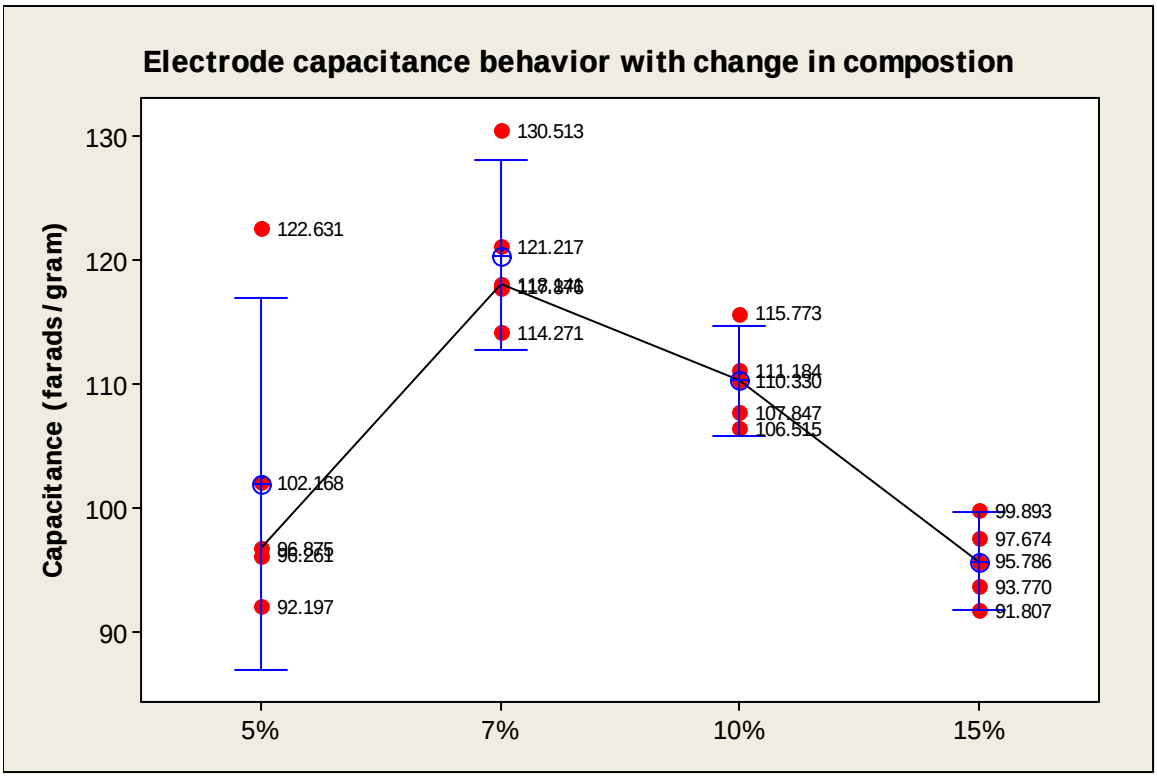

These results show that 7% conductive carbon by weight and 85% active carbon by weight is the ideal composition for optimum performance of supercapacitor electrode.

4. Conclusion

Thus, the various carbon materials for electrode were characterized to obtain the most suitable active carbon for electrode preparation. Electrode prototype was prepared with these selected materials. In the first step the capacitance measuring technique was established from which behavior of electrode was predicted for different composition. The capacitance value increased with increase in conductive carbon wt. percentage from 5 to 7% and then decreased as we increased the number further. This showed that the electrode composition of 7 % conductive carbon was the ideal one showing efficient charge discharge characteristics. The ESR behavior was also observed but the data didn't serve good due numerous factors affecting the consistency of the ESR values.

D. Ioxus Project Activities

1. Background

Ioxus, Inc. is a manufacturer of EDLC (Electric Double Layer Capacitors) devices. The principal use of these devices is for the storage of electrical energy. EDLC devices are currently used to augment battery power supplies due to their high power density or ability to deliver a great deal

of energy in a short period of time; unlike batteries their intrinsic ability to deliver energy is not limited by the underlying chemical reaction that limits the power density of a battery. This is due, in large measure to the storage mechanism used by capacitors, namely energy storage in an electric field. The extraction of that energy is very rapid and depends on a parameter known as the capacitors effective series resistance or ESR. In an ideal situation when the ESR of a capacitor is ignored the rate of power delivery is limited only by the rate at which the electric field collapses and for an ideal parallel plate capacitor this is for all intents and purposes instantaneous. In the case of actual devices it is not possible to completely eliminate ESR so that the rate of energy delivery is proportional to what is known as the characteristic time constant of the capacitor, which is the product of the ESR and the device's capacitance.

While EDLC's and capacitors in general have high power density, they have low energy density as compared to batteries. Ioxus is engaged in efforts to enhance the energy density of its product for a number of reasons, but perhaps the most important is to produce products that have energy densities that are comparable with that of batteries. This is an ambitious goal, however one that the company is working to achieve. The collaborative effort with Binghamton University is a significant part of that goal.

The project's goal is to develop what is known as a hybrid or asymmetric EDLC capacitor, which differs from its more traditional counterpart by virtue of dual or hybrid energy storage mechanisms; the hybrid has, in addition to electrostatic storage, a reversible redox (Reduction-Oxidation) reaction that stores energy as chemical potential energy. The advantage of this new structure is that it gives a device significantly increased energy density and very nearly the same power density of its more traditional counterpart.

In the parlance of electrochemistry EDLC devices store energy using either ion adsorption (EDLC field storage) or fast surface redox reactions, the latter being commonly referred to as pseudo-capacitance. The use of nano-materials and a better understanding of charge storage mechanisms within the structures that compose the electrode have led to significant increases in energy density of the electrode. Ioxus is in the process of developing an electrode using proprietary materials and techniques to take advantage of nano-structures within specially developed carbon electrode material to develop an enhanced electrode that will have a higher energy density than company's current electrode material due to the pseudo-capacitance of the electrode material.

2. Final State of Development

Ioxus has worked with Binghamton University to review various characteristics of EDLCs and Hybrid Capacitors, including thermal properties, electrode material deposition, electrolyte impurity levels, and separator properties. Raw materials were studied for various properties, as well as mixing and deposition techniques.

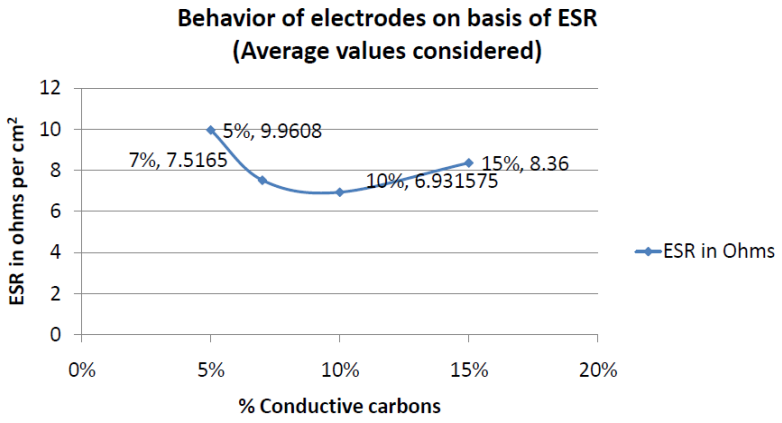

Scanning Electron Microscope (SEM) tests were performed, as well as a number of other test methods to determine how the various materials work together, and how these different materials interact together.

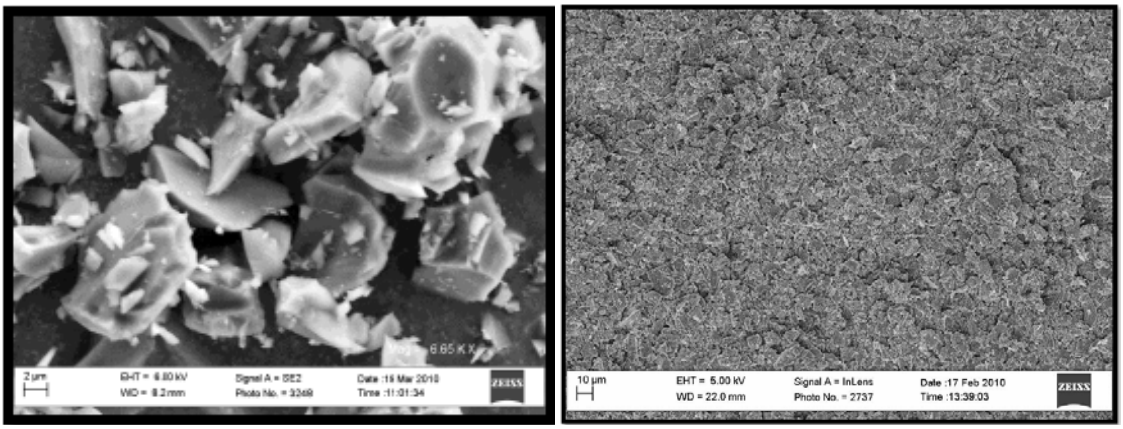

After using the tests provided by Binghamton University, Ioxus was able to use this information to create a higher energy density product, thus enhancing the energy density of a traditional EDLC and create hybrid capacitors. The thermal studies performed on traditional EDLCs allowed Ioxus to study the temperature effects of the charge/discharge cycles, and generate better designs for high power applications.

Ioxus created, enhanced, and then generated a product line of hybrid capacitors which now range in size from 220 Farads (F) to 1000F. These products have successfully been proven to work as the primary energy storage method for LED lighting applications, and two significant commercial applications are evaluating these devices for use. Both of these applications will be used in LED lighting, which replaces traditional batteries and allows for a very fast charge and a high cycle life, over a wide temperature range. This will lead to a significant reduction of waste that ends up in landfills. These products are 70% recyclable, with a 10 year life. In one both

applications, it is expected that the hybrid capacitor will power the LED lights for the life of the product, which would have required at least 10 battery changes.

Thermal and cycle testing allowed Ioxus to develop a second generation of products for high power applications. While this product is not currently commercially available, Ioxus is in the final design stages of this product line, which will be released in 2011. It is expected that the high power capability (up to 4x over currently available EDLCs) will further expand the EDLC market, as less cells will be required for high power applications.

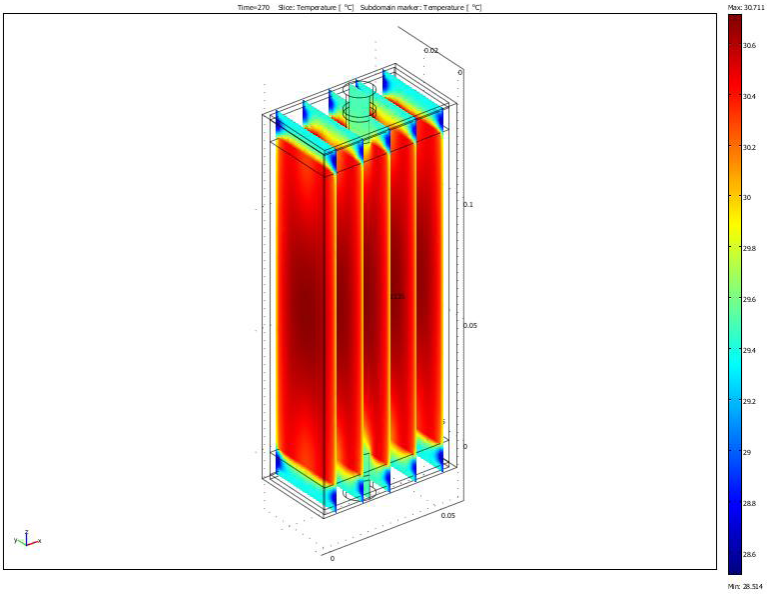

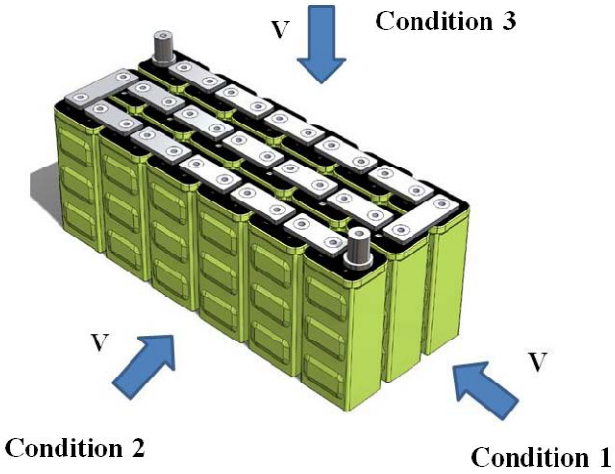

Ioxus is proud to have worked with Binghamton University in this project, and looks forward to future potential EDLC or hybrid capacitor work together.

IV. Products Developed and Technology Transfer

Publications:

"Multiphysics approach to modeling supercapacitors for improving performance" was submitted for publication in InterPACK 2011 conference proceedings, submitted for publication. Interpack 2011.

Networks Fostered:

This project launched a new research collaboration with Ioxus, Inc., in Oneonta, New York. As a result of this collaboration, Ioxus joined Binghamton University's Integrated Electronics Engineering Center, a New York State Center of Advanced Technology, where they participate in research related to electronics packaging.